

Diploma Thesis

CLASSIFICATION OF URBAN AREAS USING AIRBORNE FULL-WAVEFORM LASER SCANNING DATA

Executed at

Institute of Photogrammetry and Remote Sensing
Vienna University of Technology.

Supervised by

Ao. Univ.Prof. Dipl.Ing. Dr.techn **Josef Jansa**

and

Univ.Prof. Dipl.Ing. Dr.techn **Norbert Pfeifer**

Sharif Hasan
Vegagasse 20, 666p
1190 Wien

Vienna, May 2011

.....

Contents

1	Introduction	8
1.1	Urban planning.....	8
1.2	Classification of urban areas:.....	9
2	Airborne Laser Scanning	11
2.1	Principles of airborne laser scanning:	11
2.2	Georeferencing :.....	13
2.3	Airborne full-waveform laser scanning data:	14
2.3.1	Analysis of the full-waveform information:	16
3	ALS vs. Photogrammetry	20
4	Related work	21
4.1	Utilizing LiDAR only (Multi-Pulse systems):	21
4.2	Utilizing LiDAR data and multi spectral aerial or satellite images:	22
4.3	Utilizing only full-waveform lidar data:	24
5	Study area and data	27
5.1	Study area	27
5.2	Data Acquisition	28
5.3	Test area:	28
6	Workflow and strategy	30
6.1	Classification methods:.....	30
6.2	Hardware and software:.....	33
6.3	Features extraction:	34
6.3.1	Geometrical features:	35
6.3.2	Echo-based features.....	40
6.3.3	Physical features:.....	41
7	Feature selection and classification accuracy	44
7.1	Determining training areas and their analysis:.....	44
7.2	Classification and accuracy assessment:	49
8	Classification of the entire area	63
8.1	Maximum-Likelihood and Minimum-Distance classification:	63
8.2	Results and accuracy assessment:	65

8.3	Decision Tree classification:.....	69
9	Conclusion and further works.....	72

Acknowledgments

I would like to thank all my colleagues who supported me during the study period. Above all I would like to thank Prof. Dr. **Josef Jansa** for his continuous support and advice in many different matters concerning this thesis, and Prof. Dr. **Norbert Pfeifer** for his support and advices during my study and this thesis. Furthermore I would like to thank Dr. Markus Hollaus, Dr. Gottfried Mandlbürger, Dr. Cammillo Ressler for their help in some parts of the work.

Special thanks for my family, my father, my mother and my brothers and sister. Special thank for my love Layal! Thanks for supporting and believing in me! Thanks for all support throughout my study.

Abstract

Airborne laser scanning (ALS) data is increasingly used for classification purposes, and preferred over traditional aerial photogrammetric techniques in particular in vegetated areas. This thesis deals with the potential of full-waveform airborne laser scanning data for classification of urban areas. Information derived from full-waveform ALS data, such as amplitude and echo-width, can be used to calculate additional attributes such as backscatter cross-section. These physical attributes together with derived geometrical attributes like the normalized digital surface model, standard deviation of elevation, surface slope and the echo-based feature number of echoes are used for the classification of urban areas. The study area is located in Vienna city where four classes are to be distinguished. They are buildings, trees, roads and grass area. Three classification methods are used, which are Maximum-Likelihood, Minimum-Distance and Decision Tree. A comparison of the results of these three methods proves the potential of features extracted from full-waveform airborne laser scanning data for classification purposes in urban environment. It turns out that the achieved accuracy of the Decision Tree classification is better than that of Maximum-Likelihood and Minimum-Distance. For Maximum-Likelihood and Minimum-Distance classification, minimum amplitude of last echoes is of less importance, although it may be responsible for a slight improvement for roads and trees. Minimum echo width of last echoes is of less importance. But it has been seen that the minimum amplitude of the last echoes and backscatter cross-section are very useful for roads and grass areas classification using Decision Tree method.

Zusammenfassung

Airborne Laserscanning Daten werden zunehmend zum Zwecke der Klassifizierung verwendet, und wobei sie, vor allem im Bereich mit Pflanzenbewuchs, im Vergleich zu herkömmlichen photogrammetrischen Techniken, bevorzugt zum Einsatz kommen. Diese Masterarbeit beschäftigt sich mit dem Potenzial der Full-Waveform Laserscanning Daten für die Klassifizierung des städtischen Raums. Weitere Information ist aus Full-Waveform ALS Daten ableitbar, wie Amplitude und Breite der Echos, die dann zum Berechnen der Backscatter Cross-section (Streu-Querschnitt) verwendet werden können. Diese physikalischen Eigenschaften zusammen mit abgeleiteten geometrischen Eigenschaften wie normalisiertes Oberflächenmodell, Standardabweichung der Höhe, Geländeneigung und das echo-basierte Merkmale Anzahl der Echos werden für die Klassifizierung eines Stadtgebiets verwendet. Das Untersuchungsgebiet liegt in der Stadt Wien und vier Klassen sollen unterschieden werden. Diese Klassen sind Gebäude, Bäume, Straßen und Grassflächen. Drei Klassifizierungsverfahren werden eingesetzt: Maximum-Likelihood, Minimum-Distance und Decision Tree. Ein Vergleich der Ergebnisse dieser drei Methoden weist auf das Potenzial der von Full-Waveform Airborne Laserscanning Daten extrahierten Merkmale für die Klassifizierung von städtischem Gebiet hin. Es wird auch gezeigt, dass die Genauigkeit der Ergebnisse der Decision Tree Klassifizierung höher ist als jene der Maximum-Likelihood und der Minimum-Distance. Für die Maximum-Likelihood und Minimum-Distance Klassifizierung war die minimum Amplitude der letzten Echos von geringerer Bedeutung, obwohl es vielleicht für leichte Verbesserung für Straßen und Bäume verantwortlich zeichnet. Die minimale Echo-Breite der letzten Echos hat geringere Bedeutung. Aber es zeigte sich, dass die minimum Amplitude der letzten Echos und der Backscatter-Querschnitt sehr nützlich für Straßen- und Grassflächenklassifizierung mit der Decision Tree Methode sind.

List of Acronyms:

ALS	Airborne laser scanning
LiDAR	Light detection and ranging
FWF	Full-waveform
DTM	Digital terrain model
DSM	Digital surface model
nDSM	Normalized digital surface model
Ne	Number of echoes
Min. A	Minimum amplitude
Min. ew	Minimum echo-width
S	Slope
OPALS	Orientation and Processing of Airborne Laser Scanning data, Software toolbox developed at I.P.F.
I. P. F.	Institute of Photogrammetry and Remote Sensing, Vienna University of Technology.
WWW	World wide web

1. Introduction

1.1 Urban planning

Urban and regional planners require nearly continuous acquisition of data to formulate governmental policies and programs. These programs might range from the social, economic and cultural domain to the context of environmental and natural resource planning. There is an increased need for planning agencies to have timely, accurate and cost-effective sources of data of various forms [32].

Knowledge of land use and land cover is important for many planning and management activities. The term land-cover relates to the type of features present on the surface of the Earth (e.g. corn fields, lakes, trees, etc). The term land-use relates to the human activity or economic function associated with a specific piece of land (e.g. single-family houses, parking sites, etc). For a long time and still the aerial photos and satellite images are used for classification purposes and land-cover/use mapping. Urban land-cover classification is an important research topic in urban studies, especially with expanding urban populations around the world [12], above that the analysis of urban areas or cities has become one of the most important research topic in remote sensing community because of the complexity of various man-made or natural objects, in additional of the large range of applications in the field of urban planning and infrastructure and environment, change detection, housing, transport, telecommunications, disaster management, tourism, navigation and archiving architectural heritage etc.

The spatial resolution has increased with the progress of technology for obtaining high resolution aerial and satellite images and thus the potential to detect finer structures. Therefore urban structures such as man-made constructions, roads, or vegetated areas can be characterized more precisely, and used as input for Geographical Information Systems or for automatic mapping purposes. Airborne laser scanning (ALS) became one of the important acquisition techniques, which deliver invaluable data that can be used for object classification and parameter estimation for several fields such as in forestry and in urban applications [46]. Figure 1 shows simply an urban mapping process from airborne or space-borne images to cadastral mapping.



Figure 1. Urban mapping, Vienna city. From [62]

1.2 Classification of urban areas

Urban landscapes are composed of diverse materials (concrete, asphalt, metal, plastic, glass, water, grass, shrubs, trees, and soil) arranged by humans in complex ways to build housing, transportation systems, utilities commercial building etc. The goal of this construction is usually to improve the quality of life. To analysis urban areas and to characterize urban phenomena it is necessary to obtain data, which has appropriate temporal, spectral and spatial resolution characteristics. For decades, large-scale aerial photos and satellite images have been employed to obtain such information by applying the principles of photo interpretation [20]. For land cover/use classification purposes in urban areas many techniques have been developed and tested on remotely sensed imagery. Interpretation using texture, context, and spatial configurations of urban land cover features and multispectral classification methods have been used. Aerial photography, mainly as orthophoto, and very high spatial resolution satellites images (Ikonos and Quickbird) provide the opportunity to obtain information at large scales for urban areas. urban mapping is challenging because of the complexity and quantity of data needed to represent large urban areas and the complex morphology of cities and the varied materials used in structures [16]. However, image noise, lighting conditions (presence of shadows is often unavoidable), occlusions and scene complexity complicate the identification of urban objects.

Some authors used multi-temporal and multi sensors data sets with different acquisition geometries to provide useful approach to improve the classification results in shadows area in urban areas [15] but it may introduce errors in the classification because of different time of points. In addition to that, satellites which provide high spatial resolution, have limited spectral and temporal resolution.

Another data acquisition source for urban mapping are SAR (Synthetic Aperture Radar) images, small-baseline, long time scale coherence images (months to years) can be used to discriminate between urban and non-urban areas, and allowing basic information on urban extent to be retrieved a sequence of such observations can be used to automatically detect urban change. Digital elevation models derived by interferometry have been used to retrieve buildings height [18]. [53] used a few-meters-resolution synthetic aperture radar (SAR) images to extract the road network in dense urban areas.

SAR image processing is commonly recognized as a hard task because of high dynamics and multiplicative noise, which prevent the use of classical image processing tools. There are understandable reasons for the limited use of SAR data for land-cover classification, such as the special SAR geometry (which results in the undesired presence of shadow, layover, and fore shorting phenomena in the images), the complicated scattering process, and the presence of speckle noise. Above that it is generally difficult to obtain high classification accuracies if only one single-channel single-polarization SAR image is considered [6].

Airborne laser scanning (ALS) is an active remote sensing technique providing direct range measurements between the laser scanner and the Earth's topography. The high degree of automation in both, capturing and processing the data, and high accuracy and point density, and low cost have caused LiDAR (Light detecting and Ranging) to be preferred over traditional aerial photogrammetric techniques. The backscattered echoes from objects are detected leading to a 3D cloud of points, which stem from a mixture of terrain, vegetation, building roofs, vehicles and other natural and man-made objects, therefore, ALS became also very useful for classification of urban areas.

Since 2004, new ALS commercial systems called full-waveform lidar have appeared with the ability to record the complete waveform of the backscattered signal echo [35]. This development of full-waveform (FWF) ALS-data provide in addition to range measurements other attributes namely echo amplitude, echo width and information on multiple echoes from one shot [35] [46]. Airborne laser scanning is commonly used for high resolution digital terrain model (DTM) derivation [7], and related applications like detection of urban changes or monitoring environmental phenomena. For urban mapping, the development of full-waveform LiDAR offers the opportunity to obtain more details and properties about the illuminated surface, which leads to more reliable and accurate classification results.

2 Airborne Laser Scanning

2.1 Principles of airborne laser scanning:

Airborne laser scanning (ALS) is an active remote sensing technique providing direct range measurements between the laser scanner and the Earth' topography (Figure 2).

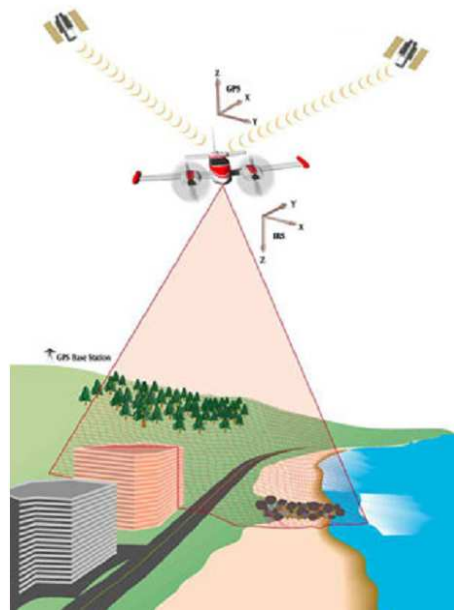


Figure 2. Airborne Laser Scanning. From [66]

Different principles can be used to measure the distance between sensor system (Laser scanner) and target. This measurement of distance or range, which always based on the precise measurement of time, can be carried out using one of the two main methods [49] [41]:

- **Pulse round trip time:**

The laser ranging instrument measures the precise time interval that has elapsed between the pulse being emitted by the laser ranger located on airplane or satellite and its return after reflection from a ground object (Figure 3, Eq. 1).

$$R = v \cdot t/2 \quad (1)$$

Where:

R is the slant distance or range
 v is the average group velocity of light
 t is the measured time interval

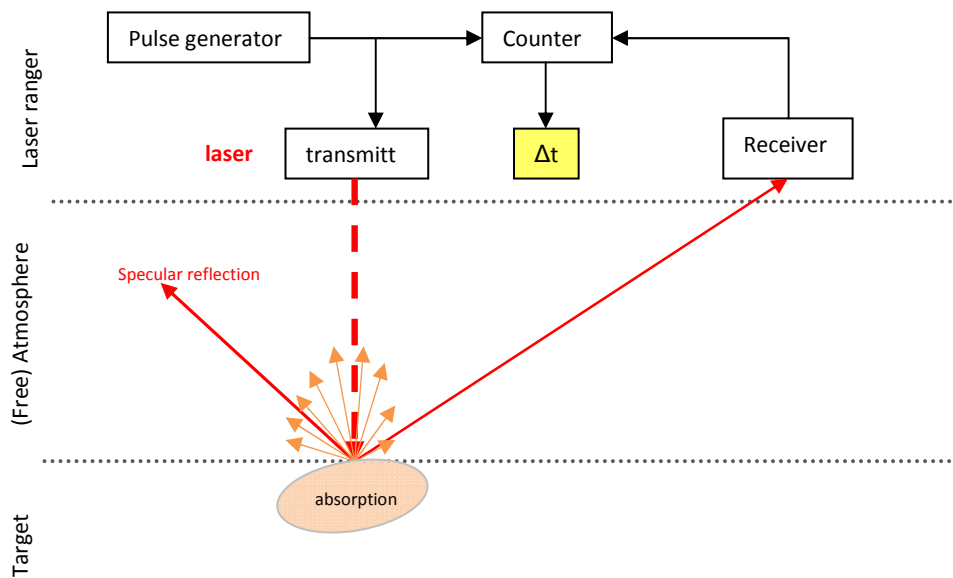


Figure 3. Principle of a pulse laser ranger, adapted from [41].

• **Phase shift measurement:**

In the second (alternative) method the laser transmits a continuous beam of laser radiation instead of a pulse. In this case, the range value is derived by comparing the transmitted and received versions of sinusoidal wave pattern of this emitted beam and measuring the phase difference between them (Figure 4, Eq. 2).

$$R=(M\lambda + \Delta\lambda)/2 \quad (2)$$

Where:

- M is the integer number of wavelengths
- λ is the known value of the wavelength.
- $\Delta\lambda$ is the fractional part of the wavelength = $(\phi/2\pi) \cdot \lambda$, where ϕ the phase angle.

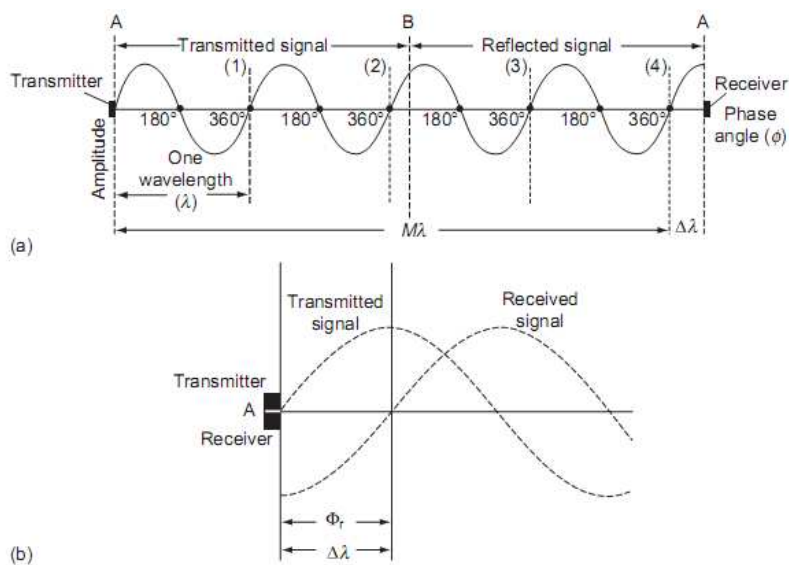


Figure 4. (a) Phase comparison is carried out between the transmitted and reflected signals from a CW laser and (b) phase comparison between the two signals takes place at the laser rangefinder located at A [49].

The largest ranges can be probed using the pulse round trip time measurement principle obtaining cm-accuracy. Shorter distances, e.g. up to 100m, can be measured faster and more accurate with the phase-based measurement technique [41].

One of the ALS-system's components is an optical scanning mechanism, it uses an optical element such as a rotating plane or polygon mirror or a fiber optic linear array to send a stream of pulses of laser radiation at known angles and at high speed along a line crossing the terrain in the lateral or cross-track direction relative to the airborne platform's flight path (Figure 5) [49].

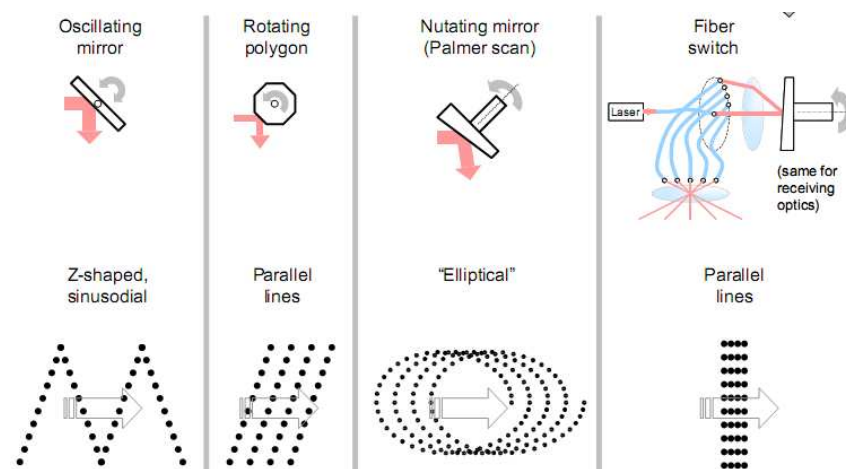


Figure 5. Scanning techniques of different ALS systems. From [8].

2.2 Georeferencing :

A laser scanner records polar coordinates, range R and scan angle α , of ground points in its own local coordinate system [29]. The combination of the GNSS (Global Navigation Satellite System) receiver and an inertial measurement unit (IMU) is the most common equipment for direct georeferencing. GPS antenna is mounted on top of the aircraft and the IMU is rigidly mounted to the sensor platform [41]. In airborne laser scanning data are acquired stripwise. For transforming laser scanner strips in the national ground survey coordinate system DGPS and IMU are used, for which only one ground reference station with ground-survey coordinates is needed [29].

The mathematical model expressed by the position of the antenna phase center (X_0, Y_0, Z_0) and the sensor attitude angles ω , ϕ , and κ to the ground point (X, Y, Z) is (Eq.3):

$$\begin{pmatrix} X \\ Y \\ Z \end{pmatrix} = \begin{pmatrix} X_0 \\ Y_0 \\ Z_0 \end{pmatrix} + R_{\omega\phi\kappa} \left(t + R_m \begin{pmatrix} 1 & 0 & 0 \\ 0 & \cos \alpha & \sin \alpha \\ 0 & -\sin \alpha & \cos \alpha \end{pmatrix} \begin{pmatrix} 0 \\ 0 \\ -r \end{pmatrix} \right) \quad (3)$$

Where:

t GPS antenna offset

R_m IMU misalignment

$R_{\omega\phi\kappa}$ Rotation matrix accounting for the rotation of the body frame to global frame.

The component GPS, IMU, and laser scanner have to be synchronized. After the direct georeferencing process the laser scanning, high precision can be achieved by applying the so-called method of strip adjustment [41] [29]. Georeferencing process provides dense and irregular distributed points (points cloud) in an identified coordinate system (e.g. WGS84). Depending on the geometry of illuminated surfaces, several backscattered echoes may be recorded for a single emitted pulse. Such systems are called multiple pulses or multi-echo LiDAR sensors [39].

2.3 Airborne full-waveform laser scanning data:

The new technology of full-waveform (FWF) LiDAR has the ability to record the complete waveform of the backscattered signal echo. Thus, in addition to the basic geometric representation of the Earth topography, it provides physical properties of the observed targets. "Waveform", refers to the shape of the return signal, whose analysis allows one to set up advanced processing methods which increase pulse detection reliability, accuracy and resolution [35].

Decomposing the waveform into a sum of components or echoes maximizes the detection rate of relevant peaks, thus characterizing the different targets along the path of laser beam, and generating a dense 3D point cloud (Figure 6) [55] [35].

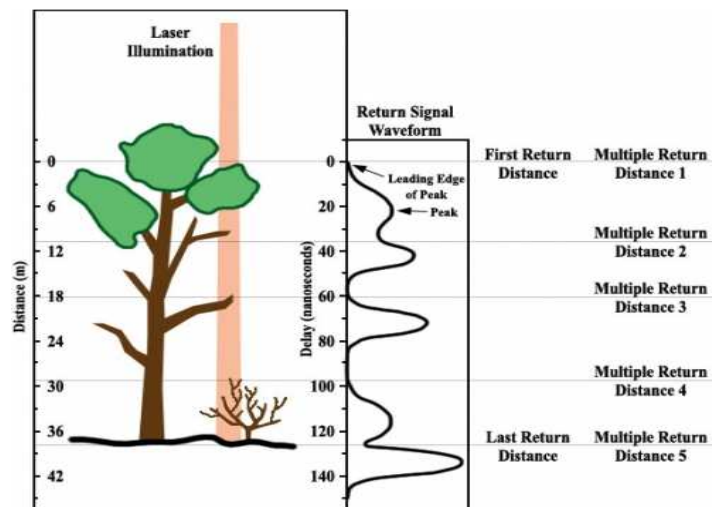


Figure 6. Multiple echoes recorded by FWF-ALS data analysis. From [67].

Additional properties can be extracted by modeling the waveform as series of Gaussian pulses, for each echo characteristics properties can be easily derived, which describe the shape of the echoes, such as amplitude and echo width [55]. The amplitude is a measure of the strength of the echo. The echo width could refer either to the full width at half the amplitude, or to the standard deviation of the decomposed Gaussian-shaped echo (Figure 7).

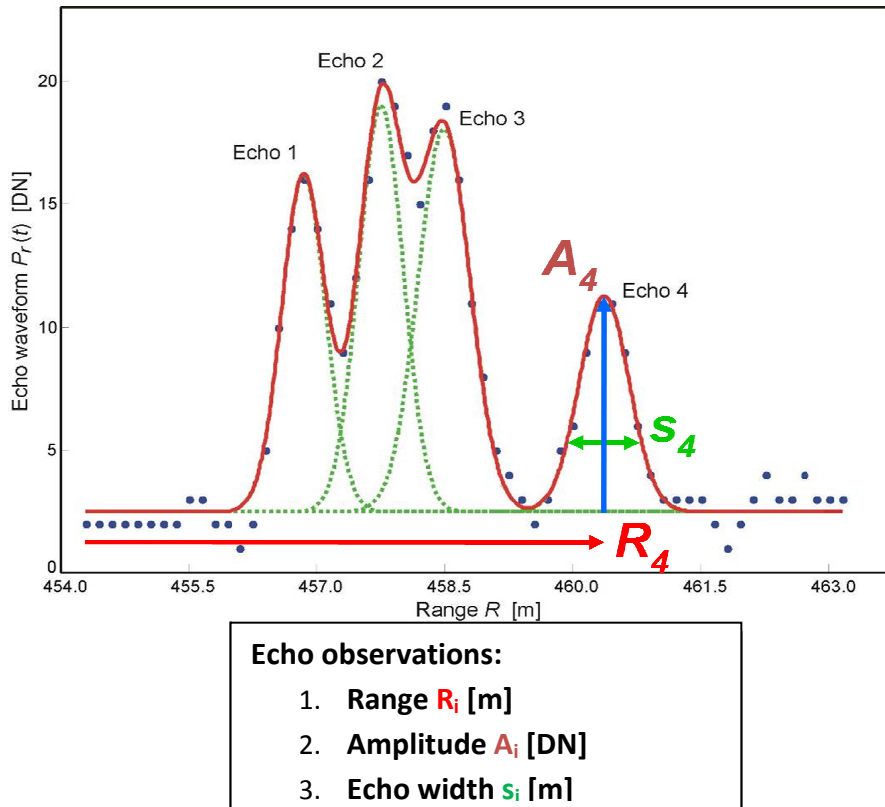


Figure 7. Geometric and radiometric information per echo. From [24].

Full-waveform topographic LiDAR systems mainly differ in footprint size, pulse energy and PRF (Pulse Rate Frequency). Small-footprint and large-footprint systems don't collect the same information over the same area (Figure 8). Therefore the applications differ from system to another [33]. Most commercial systems are small-footprint (0.2-3m diameter depending on flying height and beam divergence) with higher PRF. They provide a high point density (more than 100 p/m² in some specific applications) and an accurate altimetric description within the diffraction cone, therefore it is suitable for topographic mapping and other terrestrial applications.

Small-footprint systems often miss tree tops and it is difficult to determine whether the ground has been reached in dense vegetation [35]. Large-footprint systems (10-70m diameter) increase the probability to both hit the ground and canopy top. The first experimental full-waveform topographic systems were large-footprint and mostly carried by satellite platforms. Such as the Airborne Laser Vegetation Imaging

Sensor (LVIS) or the Geoscience Laser Altimeter System (GLAS) flown on board the ICESat satellite [57] [35].

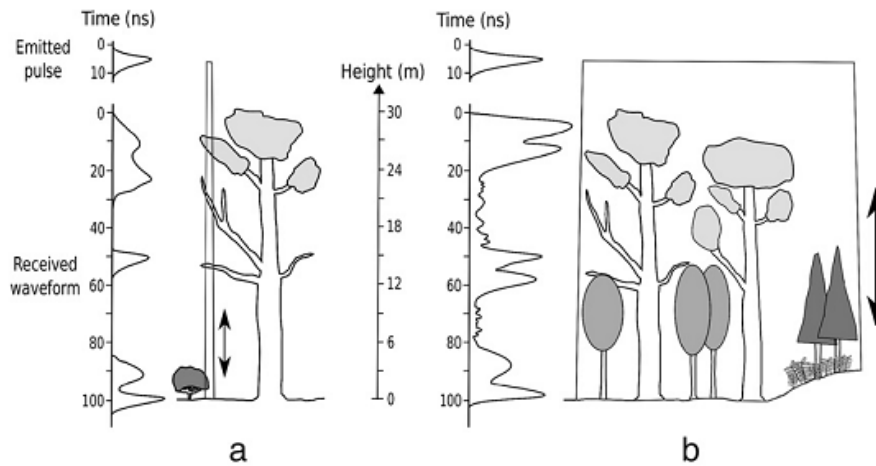


Figure 8. (a) a small-footprint LiDAR and (b) a large-footprint LiDAR. From [35].

2.3.1 Analysis of the full-waveform information:

Wagner, et al [55] have used radar equation adapted to ALS to describe the shape of echo waveform which depends on the emitted laser pulse and the backscattering properties of the target (Figure 9).

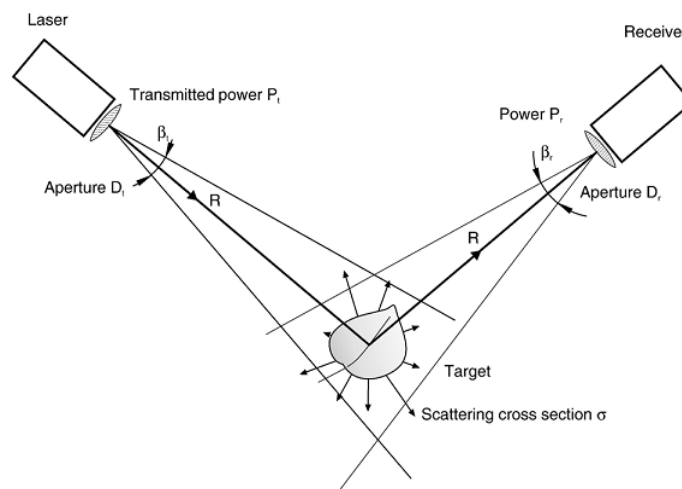


Figure 9. Geometry and parameters involved in the radar equation. Unlike a real hardware setup, transmitter and receiver are drawn separately. From [55].

By combining all target parameters into one parameter, the backscatter cross-section σ can be obtained:

$$\sigma = \frac{4\pi}{\Omega} \rho A_s \quad (4)$$

Where:

ρ the reflectivity
 A_s the receiving area of scatterer
 Ω cone of solid angle.

The backscattering characteristics of a target depend on its size, its reflectivity and the directionality of scattering.

2.3.1.1 Gaussian decomposition:

For spatially distributed targets the return signal is the superposition of echoes from scatterers at different ranges or time. Scatterers produce distinct echoes if separated by distances larger than the range resolution of ALS system [55]. The recorded signal $P_r(t)$ by the receiver of a small-footprint waveform ALS system is the result of a convolution of the transmitted pulse and differential cross-section multiplied by the term $1/R^4$, the recorded waveform can be described by a formulation of radar equation adapted for ALS:

$$P_r(t) = \sum_{i=1}^N \frac{D_r^2}{4\pi R_i^4 \beta_i^2} \eta_{sys} \eta_{atm} S(t) * \sigma_i(t) \quad (5)$$

Where:

P_r received signal power [W]
 S system waveform [DN]
 D_r diameter of receiver aperture [m]
 R Range from sensor to target [m]
 β laser beam divergence [rad]
 η_{sys} system transmission factor [-]
 η_{atm} atmospheric transmission factor [-]
 σ backscatter cross section [m²]

the system waveform $S(t)$ of the laser scanner defined as the convolution of the transmitted pulse $P_t(t)$ and the receiver response function $\Gamma(t)$:

$$S(t) = P_t(t) * \Gamma(t) \quad (6)$$

In practice, $P_t(t)$ and $\Gamma(t)$ cannot be easily determined independently [55]. This system waveform and the scattering properties of a cluster of scatterers can be described by Gaussian function:

$$S(t) = \hat{S} e^{-\frac{t^2}{2s_s^2}} \quad (7)$$

Where:

\hat{S} amplitude
 s_s the standard deviation.

In order to come to an analytical waveform solution, it will be assumed that the scattering properties of a cluster of scatterers can be described by a Gaussian function:

$$\sigma_i' = \hat{\sigma}_i e^{-\frac{(t-t_i)^2}{2s_i^2}} \quad (8)$$

Where:

- $\hat{\sigma}$ amplitude
- s_i standard deviation of the cluster (echo) i
- t_i position of cluster i

then the final result is to decompose the received signal into several Gaussian curves:

$$P_r(t) = \sum_{i=1}^N \hat{P}_i e^{-\frac{(t-t_i)^2}{2s_{P,i}^2}} \quad (9)$$

Where:

- t_i round trip-time
- $s_{P,i}$ standard deviation (echo width) of the echo pulse i
- \hat{P}_i Amplitude of echo i

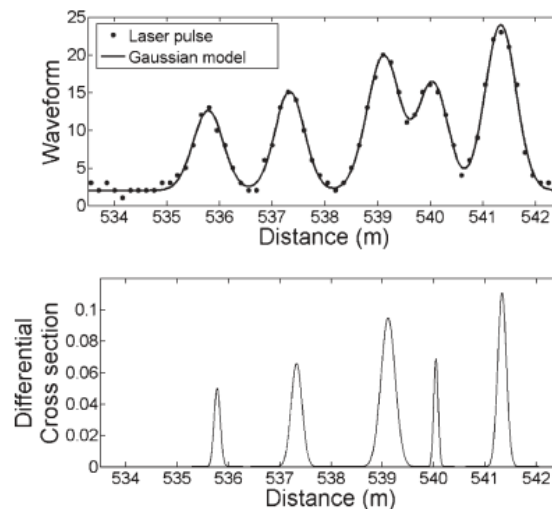


Figure 10. Example of a measured versus the modeled waveform (top). The bottom figure shows the corresponding cross-section profile in $m^2 m^{-1}$. From [55].

2.3.1.2 Radiometric calibration:

These physical observables (amplitude, echo width) are influenced by many different factors (e.g. range, angle of incidence, surface characteristics, atmosphere, etc...) therefore, these attributes can hardly be used without radiometric calibration [33]. From the adapted formulation of the radar equation (Eq. 5), the parameters which

are unknown but can be assumed to be constant during one ALS campaign can be combined to one constant, the so-called calibration constant C_{cal} .

$$\sigma = \frac{C_{cal} 4\pi R^4 \hat{P}_i S_{P,i}}{\eta_{atm}} \quad \text{with } C_{cal} = \frac{\beta_t^2}{P_t D_r^2 \eta_{sys}} \quad (10)$$

In order to estimate the C_{cal} only the backscatter cross-section of a reference surface is necessary. From (Eq. 4) and with the assumption of a Lambertian scatterer, that means $\Omega = \pi$ steradians and the knowledge of the reflectivity ρ of the reference we can easily derive the calibration constant C_{cal} . Once the calibration constant is derived, the calibrated backscatter cross sections of the individual echoes for the whole data set can be determined. Due to different flight heights or beam divergence, the illuminated area A_i (figure 11), and therefore, also the backscatter cross section σ can vary a lot. Therefore, Wagner et al [56] introduce area-normalized values, so-called backscattering coefficients (Eq. 11 and 12).

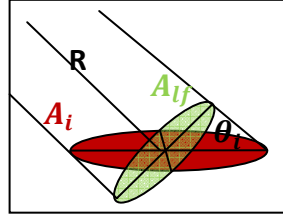


Figure 11. Laser footprint area at the scattering object A_{lf} , i.e. the circular area perpendicular to the laser beam at distance R (green area); area illuminated by the laser beam A_i at distance R and θ_i angle of incidence (red area). From [33].

- Cross-section per unit-illuminated area σ^0 [$m^2 m^{-2}$]: $\sigma^0 = \frac{\sigma}{A_i}$ (11)

- Bi-static scattering coefficient γ [$m^2 m^{-2}$]: $\gamma = \frac{\sigma}{A_{lf}} = \frac{\sigma^0}{\cos \theta_i}$ (12)

where: A_{lf} laser-footprint area at the scattering object.

The backscatter cross-section σ as well as the backscattering coefficients σ^0 and γ are not free from influences of the angle of incidence, therefore in case of ideal Lambertian scatterers further radiometric corrections are needed which are not used in this work. Further used are the backscatter cross-section σ and the bi-static backscatter coefficient γ . As one can see in equation (12), γ is just σ normalized to the laser footprint area A_{lf} . Due to the small elevations differences in our area the footprint does not vary much, thus the ratio between γ and σ will be almost constant over the entire area under investigation. Therefore, these two coefficients are highly correlated, as we shall see later.

For more details about Gaussian decomposition and calibration of FWF-ALS data please read [33] [55] [56] [58] [59].

3 ALS vs. Photogrammetry

Optical sensors record passive solar or artificial radiation backscattered by objects in the camera's field of view in different wavelength bands, while laser scanner records the backscattered radiation for one wavelength only (commonly near infra-red). Therefore the task of classification of land-cover/use in urban areas using only ALS-data is facing some difficulties. Some authors have used additional information from aerial images as in [3] [9] [12] [40] [51] [60]. From LS sensors, which record the entire wave, not only geometric properties of the targets can be delivered but also further physical properties, like amplitude, echo-width and cross-section, which may improve classification from ALS-data.

The most important advantages of ALS are [5] [23]:

- Mapping of surfaces with very little/no texture or poor definition.
- Not influenced by heavy cast shadows or severe brightness contrasts.
- Not influenced by light conditions, it can work after sunset and before sunrise.
- Penetration of vegetation to a certain extent.
- Dense and accurate measurements provide more accurate DSM generation of urban regions.
- Range measurements can be quickly converted to 3D coordinates which can be important in some cases, specially for monitoring natural disaster.

The integration of laser scanning and photogrammetry has been discussed in [23][31][44]. [44] wrote that the integration of laser point clouds and images can have different levels depending on the desired end-product, the main levels of integration are:

1. Object-level integration
2. Photogrammetry aided by laser scanning
3. Laser scanning aided by photogrammetry
4. Tightly integrated laser scanning and optical images.

In our work we don't meet any of these levels, we will use only FWF-laser scanning data (FWF) for the classification of urban areas.

4 Related work

Since the beginning of the use of airborne laser scanning, attempts existed to classify the 3D points cloud for mapping and modeling applications.

The work can be categorized in two directions:

1. Classification of aerial LiDAR data into terrain and non-terrain points.
2. Classification of aerial LiDAR data into classes of surface objects such as Buildings, trees, etc [9].

In the first category there has been a dramatic increase in the development of filtering algorithms over the past 15 years which strongly rely on the spatial relationship between points with the objective of generating digital terrain models. Kraus and Pfeifer and others [28][42] have used the algorithm for filtering the laser scanner data originally designed for applications in wooded areas. Their algorithm is an iterative robust interpolation, which uses a stochastic model (weight function) and functional model (Interpolation). Vosselman [54] has used slope based filter to distinguish between the laser pulses reflected on the ground surface from those reflected from buildings and vegetation. Lin et al [30] have used the pulse width as additional information from full-waveform data for a filtering algorithm in order to improve digital terrain model (DTM) creation.

We now briefly give some previous work for the 2nd category, i.e. for the classification of LiDAR data into classes. With the increasing point density of airborne laser scanning, a detailed description of the Earth's surface, especially in urban areas can be achieved, leading to more interest using LiDAR data to extract natural and man-made objects (buildings, vegetation, roads, etc) thus providing valuable information for city planning and modeling, change detection, road graph update, land-cover/use mapping.

In the following previous work on this topic will shortly be described and grouped into 3 categories depending on the data used in classification:

- Utilizing LiDAR data only (multi-pulse system)
- Utilizing both LiDAR data and multi-spectral aerial or satellite images.
- Utilizing only Full-waveform laser scanning data.

4.1 Utilizing LiDAR only (Multi-Pulse systems):

Most work in this category investigates the geometric properties and topological features extracted from 3D points cloud and/or the laser intensity to identify objects such as buildings, trees, and roads in urban area. Tarsha-Kurdi, et al [52] have used segmentation method of LiDAR point clouds focusing exclusively on the first echo only to discriminate buildings and terrain. Clode, et al [10] and Samadzadegan, et al

[50] have described different methods for the detection of roads from LiDAR data using both height and intensity information. Rutzinger et al [43] have presented a segmentation approach which follows the principle of object-based point cloud analysis for the detection of high vegetation in urban areas. Point features used are e.g. roughness, the ratio between 3D and 2D point density, or statistics on first and last echo occurrence within the segments.

Sithole, G. et al [47] have presented an algorithm for detecting bridges in points cloud. Carlberg, M. et al [13] have introduced a multi-category classification system for identifying water, ground, roof and trees in airborne LiDAR data using 3D shape analysis (Figure 12). Bernnan. R, et al [4] have used height and intensity data to classify land cover using an object-oriented approach.

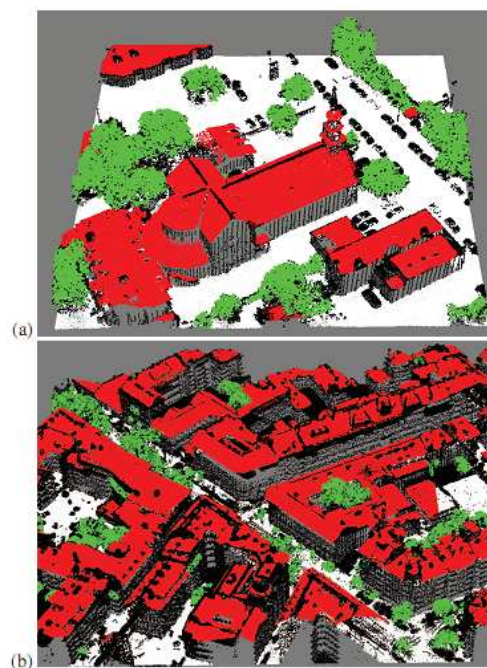


Figure 12. Classified LiDAR points cloud using 3D shape analysis. From [13].

4.2 Utilizing LiDAR data and multi spectral aerial or satellite images:

As mentioned in chapter 3, LiDAR data may be integrated in combination with imagery. The focus here is on the analysis of ALS point cloud, though image data provide additional information [44].

Airborne laser altimetry and high resolution remotely sensed imagery data offer exciting possibilities for feature extraction and spatial modeling in urban areas [60]. Properly integrating laser scanning with image data allow us to compensate individual weaknesses of each method alone (imagery: e.g. shadows, occlusion, ALS-data: e.g. spatial resolution, edge definition).

Mancini, A. et al [40] have presented an automatic approach to object extraction in urban area (buildings, grass, land and tree then at the end roads) based on different stages by using both LiDAR (the height difference between the last pulse DSM and the DTM and the height difference between the first pulse and the last pulse DSM) and multi-spectral high resolution data (R, G, B, NIR and NDVI) using AdaBoost classification algorithm (Figure 13). Charaniya, A. et al [9] have used five features (ALS data: Normalized height, height variation, multiple returns and intensity and the fifth feature is luminance from aerial imagery) to classify data sets into trees, grass, roads and roofs (Figure 14). Zhan, Q. et al. [60] have used combination of high spatial resolution airborne LiDAR data and Ikonos imagery data in urban land use classification by applying hierarchical image objects and structural image analysis techniques. Bartels, M. and Wei, H. [3] have used a supervised classification algorithm based on maximum likelihood, using first, last echo DSM and LiDAR intensity data and aerial photo in visible and near infrared (NIR) spectrum.

Chen, Y et al. [12] have used Quickbird imagery and LiDAR data to extract nine kinds of urban land cover objects. Tooke, Th. et al [51] have classified urban vegetation using an approach based on spectral unmixing and statistically developed decision trees from high spatial resolution Quickbird imagery and LiDAR data.

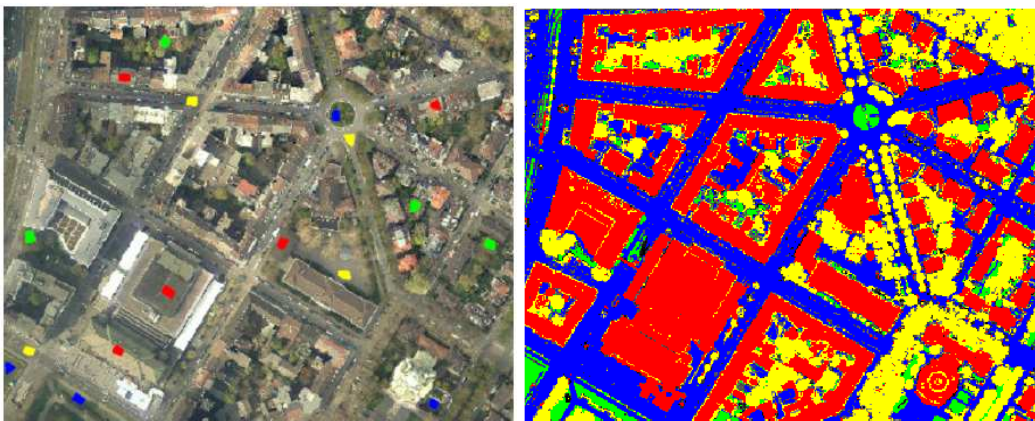


Figure 13. Left: Training Data sets, right: Result of classification using LiDAR features and spectral features: red stands for building, yellow for tree, blue for land and green for grass. From [40].



Figure 14. Classification results using LiDAR features and luminance from aerial image, left: only LiDAR features, $P(\text{correct})=0.74$, right: All features, $P(\text{correct})=0.85$. From [9].

4.3 Utilizing only full-waveform LiDAR data:

In addition to multi-echo laser scanners, full-waveform systems are able to record the complete waveform of each backscattered pulse. These systems provide more information about the structure and the physical characteristics of the targets. Few studies have focused on the use of this data only, without assistance data such as aerial images or multi-spectral images.

Some of them have focused on urban vegetation detection using full-waveform airborne LiDAR data. B. Höfle, et al [22] have presented a new GIS workflow for fully automated urban vegetation and tree parameter extraction from FWF-LiDAR data by combination of raster and point cloud-based methods. Alexander, C. et al [2] have used FWF-ALS data to evaluate the classification and extraction of vegetation characteristics for topographic mapping. The classification was undertaken on the point cloud based on the local statistical variation of attributes of TIN triangles as well as attributes of the individual points. Rutzinger, M. et al [46] have used an object-based point cloud analysis approach, combining segmentation and classification of the 3D FWF-ALS points designed to detect tall vegetation (trees and shrubs) in urban environments. They have used this approach to maintain the full resolution and information in ALS data and to avoid any rasterization and conversion to a 2.5D model. Ducic, V. et al [14] have used the additional features derived from the full-waveform data (amplitude, pulse width, and number of echoes) to discriminate between vegetation and non-vegetation points, using a Decision Tree technique, without using geometry information.

Both Alexander, C. et al [1] and Mallet, C. et al [37] have used only FWF-ALS data for supervised classification of urban areas (Decision Tree and SVM respectively). They used in addition to geometric features, physical attributes of each points extracted from FWF-ALS data. Mallet et al [37] used the generalized Gaussian (GG) model which improves the signal fitting for symmetric and distorted waveform shapes by introducing a feature parameter which modifies the shape of the peak of the Gaussian function. Figure 15 gives example of classified point over dense built-up area using SVM method. Alexander, C. et al [1] have used range and echo width for radiometric calibration and derived backscatter cross section per unit area σ^0 and the backscatter coefficient γ which are useful for separating roads and grass. Figure 16 shows the result of classification with two areas indicated where the classification failed. We can see that the bridge has been incorrectly classified as building (A), some of the points has been incorrectly classified as shrubs within roads due to their estimated elevations from the ground (A). The water body at (B) has been incorrectly classified as road. Zaletnyik, P. et al [61] have used an unsupervised classification method, using statistical parameters, such as standard deviation, skewness, kurtosis and amplitude, these four statistical parameters were used as input to the SOM (Kohonen's **S**elf-**O**rganizing **M**ap) classification to separate vegetation (trees and grass) and non-vegetation surfaces. And the range calculated from the center of mass of the waveform was used to separate the non-vegetation surface into pavement and roof categories.

From previous works, we find that most of them have been using geometric features extracted from ALS-data (multi-pulses systems) or additional data derived from aerial photographs. Most works that used only FWF-ALS features have focused only on urban vegetation detection for topographic mapping purposes. But few works have used these features to classify urban areas into different classes.

This work will be a contribution to confirm the importance of using only features extracted from full-waveform ALS data for classification of urban areas, but by using classical supervised classification methods, like Maximum-Likelihood, Minimum-Distance and Decision Tree. This work is to investigate whether these approaches can be successfully applied for the classification of urban areas. It should also find out the best suited features for discriminating between Buildings (flat and tilted roofs), Trees (with height more than 1m), Roads (all paths for vehicles and pedestrians) and grass areas.

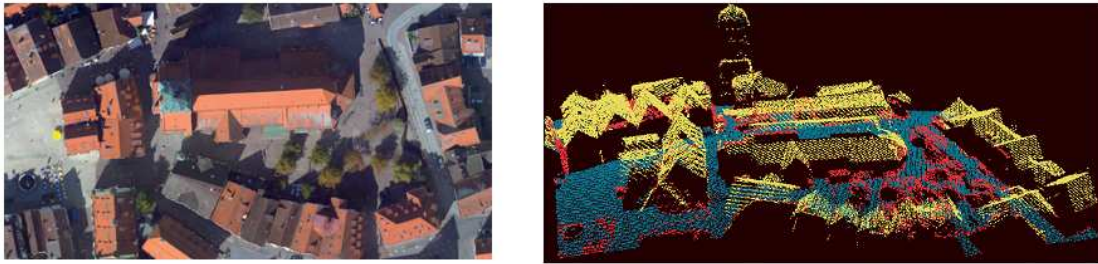


Figure 15. Classification results in a dense urban area, left: Orthophoto, right: classified point cloud. From [37].

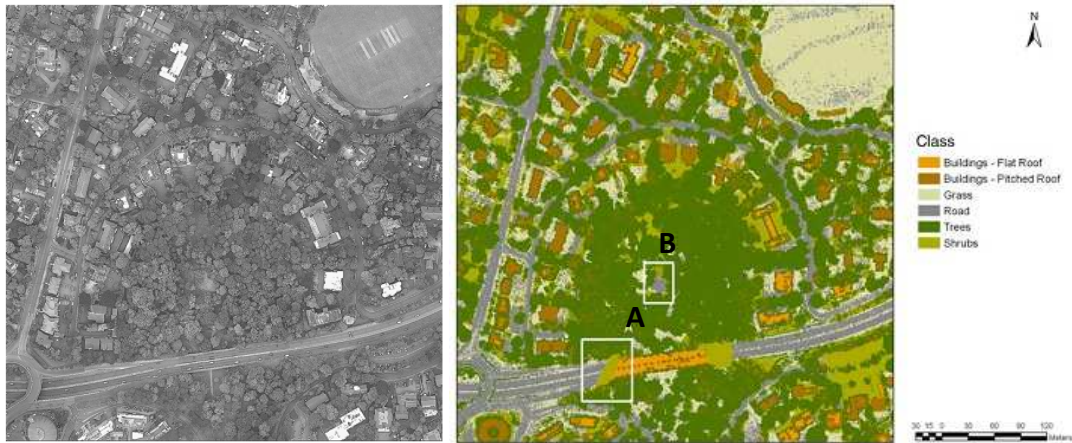


Figure 16. Left: Aerial image of study area, right: Points classified using the Decision Tree with the backscatter coefficient γ as an attribute. From [1].

5 Study area and data

The following sections provide a description of the dataset used for this thesis, starting with an overview of the study area covered by the ALS data (section 5.1), then giving detailed information about the used data and acquisition (section 5.2).

5.1 Study area

The study area is located in the center of the city of Vienna. An area of 1km X 1.36 km was chosen, defined by South-West corner in Gauss-Krüger Austrian coordinate system (1690.00 m, 340450.00 m) to the North-East corner (2700.00 m, 341810.00m), in WGS84 from (longitude 16°21' 17.81" E to 16°22' 6.52" E) to (latitude 48°12'8.77" N to 48°12' 52.82" N). This area includes a range of land use and land cover types, blocks of dense compact buildings, historical buildings (e.g. Rathaus), some gardens (e.g. Volksgarten), trees along the road, some park areas and grasslands (Figure 17).



Figure 17. Study area (red bounding box). Image from Bing maps (© 2011 Microsoft Corporation).

5.2 Data Acquisition

The available FWF ALS data are provided by the city of Vienna (MA41-Stadtvermessung) [65]. The laser scanning flight was carried out in Spring 2007 by the company Diamond Airborne Sensing GmbH using a RIEGL LMS-Q560 full-waveform scanner [63]. The ALS data cover the whole city of Vienna and some small sections across the border to Lower Austria. The LMS-Q560 full-waveform scanner uses short laser pulses with a wavelength of 1.5 μm and a pulse width of 4 ns. The laser beam divergence is 0.5 mrad and the scan angle varies between $\pm 22.5^\circ$. The flight strips have a crosswise overlap of approx. 50%. The average flight altitude was about 450 to 500 m above ground, which resulted in a theoretical laser footprint diameter of 25 cm on ground. The point density of the ALS data is an average of 15 to 20 points per square meter.

5.3 Test area:

For exploratory full-waveform ALS data classification a test site as a part of the whole study area was used. It is defined by South-West corner in Gauss-Krüger Austrian coordinate system (1700.00 m, 340900.00m) to the North-East corner (2200.00m, 341790.00m). This test area includes regular distributed buildings, some parks (e.g. Rathaus Park), some grasslands and roads (Figure 18).



Figure 18. Aerial image of the test area, from Bing maps (© 2011 Microsoft Corporation).

6 Workflow and strategy

In addition to the classification of urban areas, the aim of this work is to assess the relevance of full-waveform features by using classical supervised classification methods, like Maximum-Likelihood, Minimum-Distance and Decision Tree.

For that purpose spatial information and full-waveform features are extracted. These two kinds of features are merged into a single feature vector, input of the classification task. In order to choose the most appropriate feature set, and evaluate the relevance of full-waveform features in comparison to geometric attributes, a feature selection is considered. Performing the classification using selected features is evaluated (accuracy assessment). Consequently, conclusions can be provided for each classification method. Figure 19 illustrates the workflow, which will be followed for our objective. At the first features are extracted from FWF-ALS data. Each classification method will be applied to the selected feature vector to discriminate between buildings, trees, roads and grass areas.

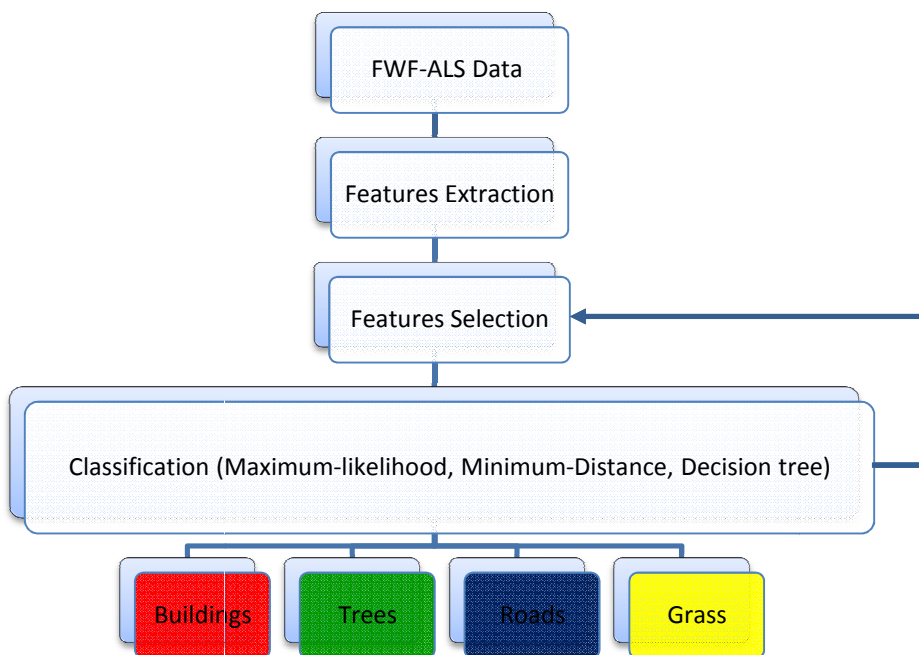


Figure 19. Workflow of the classification.

6.1 Classification methods:

Supervised classification algorithms are used to assign an unknown pixel to one of a number of classes. The choice of a particular classifier or decision rule depends on the nature of the input data and the desired output.

Applying spectral-based image classification requires rasterization of ALS data. Therefore, all extracted features are converted to raster-images with resolution of 0.5m. As mentioned in previous section, classical supervised classification methods will be used.

- **Maximum-Likelihood classifier:**

The Maximum-Likelihood classifier quantitatively evaluates both the variance and covariance of the features of the respective categories when classifying an unknown pixel. For that, there is an assumption that the distribution of the cloud of points formed by the feature vectors of training data of a category is Gaussian (normally distributed). Under this assumption, the distribution can be completely described by the mean vector and the covariance matrix. Given these parameters, the statistical probability of a given pixel is computed [32]. The probability density functions (see figure 20) are used to classify an unidentified pixel. The greatest probability density for the pixel vector decides the category to which it is assigned. After evaluating the probability in each category the pixel would be either assigned to the most likely class or if it exceeds a given probability threshold set by the analyst, will be labeled "unknown".

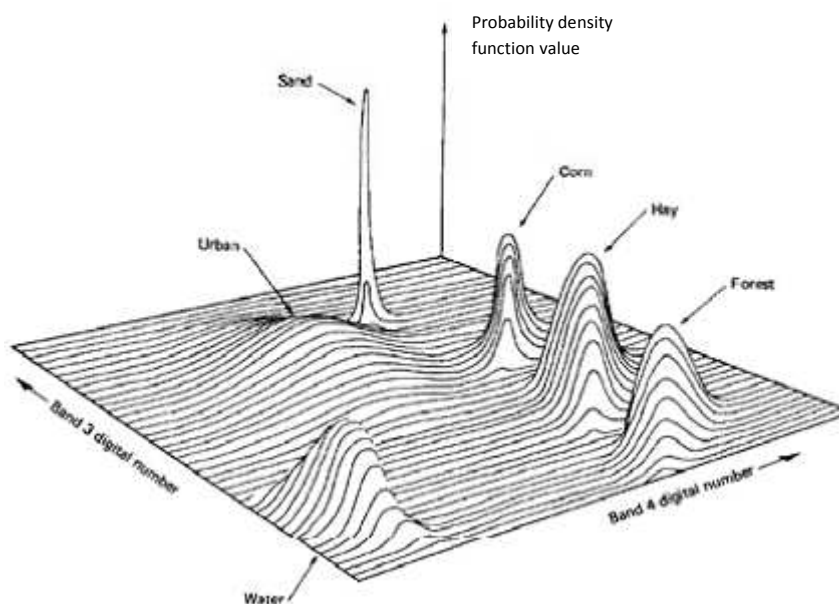


Figure 20. Probability density functions defined by a maximum likelihood classifier. From[32]

- **Minimum-Distance classifier:**

It is one of the simpler classification strategies. For each training set, which is a representative of a category (or class), the mean value of the feature vector is determined, yielding the mean vectors for each category. A pixel of unknown identity may be classified by computing the distance of its feature vector to all other

mean vectors of the categories. The unknown pixel is assigned to class of the "closest" mean vector. Pixel 1 in figure 21 would be assigned to class C.

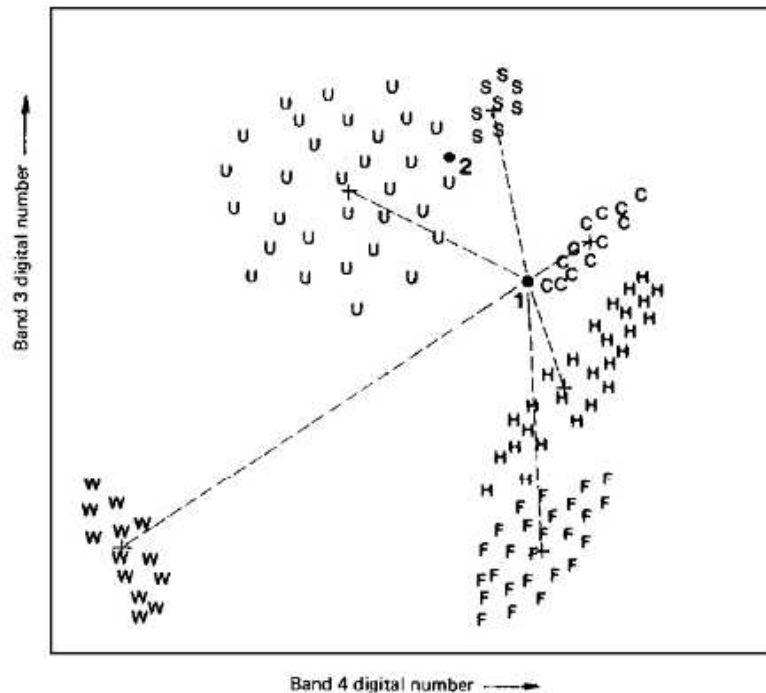


Figure 21. Minimum-Distance classifier, 1 and 2 are pixels to be classified. From [32].

- **Decision Tree:**

It is the most commonly used because of its ease of implementation and easier to understand compared to other classification algorithms. A Decision Tree is used to assign land cover classes. It is a non-parametric, hierarchical classifier which predicts class memberships by recursively partitioning a data set into more homogeneous subsets. It consists of a root (rule, consisting of conditions, apply to the initial data set), branches (progress directions after decisions), nodes (rules applied to intermediate results) and leaves (final decisions, i.e. class assignments) (Figure 22).

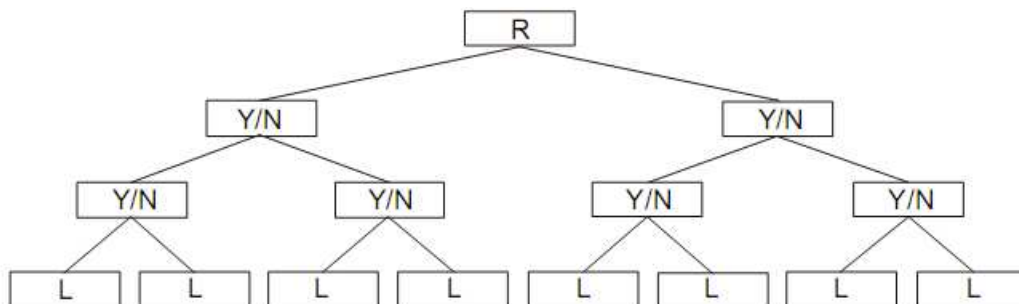


Figure 22. Decision Tree design.

6.2 Hardware and software:

The full-wave airborne laser scanning data provided for this work was processed using the hardware and software provided at the Institute of Photogrammetry and Remote Sensing (I.P.F.) at the Vienna University of Technology.

- To extract features from FWF-ALS data **OPALS software** is used.

OPALS (Orientation and Processing of Airborne Laser Scanning data) is a scientific software project developed at the Institute of Photogrammetry and Remote Sensing (I.P.F.), TU Vienna.

The aim of OPALS is to provide a complete workflow for processing airborne laser scanning data (waveform decomposition, georeferencing, quality control, structure line extraction, point cloud classification, DTM generation and several fields of application like forestry, hydrology/hydraulic engineering, city modeling and power lines) [64].

OPALS is a modular program system consisting of small components (modules), each covering a well defined task. To handle ALS data in the order of $> 10^9$ points, a central data management component (OPALS Data Manager, ODM) was developed. It provides efficient spatial data access and an administration concept for storing arbitrary point attributes (e.g. echo width, amplitude, normal vector, etc.). In our work, the modules `opalsCell`, `opalsGrid`, `opalsAlgebra` and `opalsDiff` are used.

Since ALS is a highly automated data capturing technique yielding an irregular point cloud, raster based data analysis is an important issue. Analyzing the data in a regular raster structure is an established and convenient way to retrieve summary information about the data on a per cell basis. Thus, the aim of `opalsCell` is to derive raster models by accumulating selected features (minimum, maximum, mean, etc.) of a selected input data attribute (Z, amplitude, echo width, etc.).

The aim of `opalsGrid` is to derive digital surface models (DSM/DTM) in regular grid structure using simple interpolation techniques like nearest neighbor or moving planes. In addition, additional feature models (e.g. sigma-z, slope, excentricity, etc.) can be derived simultaneously as some of them are side products of the grid interpolation and, thus, can be provided without loss of performance.

The aim of `opalsAlgebra` is to derive a new grid dataset by combining multiple input datasets. The new grid values are calculated by applying an alfabric formula using the grid values of the respective inputs grids.

The aim of `opalsDiff` is to derive difference grid models based on either two input grids or a single input grid and a horizontal reference plane.

- **GVE software v. 3.5.15** is used for view and edit laser scanning data (INPHO GmbH, Stuttgart).
- For DTM calculation **SCOP++ software v.5.4** is used. SCOP++ is designed for interpolation, management application and visualization of digital terrain data, with special emphasis on accuracy. SCOP++ has been developed and improved in cooperation of INPHO GmbH, Stuttgart and of Institute of Photogrammetry and Remote Sensing (I.P.F.) Vienna [69].
- For classification and image processing **ENVI software** is used. ENVI provides advanced, user-friendly tools to read, explore, prepare, analyze and share information extracted from all types of imagery. Classification methods are implemented in it. all ENVI solutions are built on [IDL](#) a powerful programming language.

6.3 Features extraction:

All used features are extracted only from full-waveform airborne laser scanning data.

Geometrical (spatial) features are computed just by using the 3D coordinates. They are nDSM, slope, sigma-z. By the full-waveform processing additional attributes can be retrieved thus improving the quality of these features.

Echo-based features, The echo number or the type of echo (single, first of many, intermediate, or last) may help to discriminate, especially in vegetated areas. In our work only the number of echoes will be extracted.

Physical features (full-waveform features) are obtained from the processing of the waveforms described in section 2.3.1 .

Table 1 provides an overview of the features which have been extracted and further investigated.

Geometrical features	Echo-based features	Physical features
Normalized digital surface model, nDSM	Number of echoes, Ne	Amplitude, A
Slope, S		Echo-width, ew
Sigma-z, σ_z		Gamma, γ
		Cross-section, σ

Table 1. Used features in classification.

6.3.1 Geometrical features:

6.3.1.1 Normalized digital surface model (nDSM):

nDSM is calculated by subtracting the DTM from the DSM. In urban areas the DTM describes the terrain without buildings, vegetation (trees and shrubs), in other words the bare ground and other off-terrain, often mobile objects like cars, vehicles, etc. The DSM describes the roofs and the elevation of the top most vegetation (trees and shrubs). The DSM and the DTM in urban areas are equivalent in open areas like streets, grass areas with "short" vegetation and parks areas. Therefore, the nDSM contains object heights such as building and tree heights and provides, therefore, invaluable information for classification.

- **DTM generation:**

For DTM calculation from measured points clouds, which have to be classified into terrain and off-terrain echoes (filtering), robust filtering algorithm is used [28]. The standard DTM generation procedure implemented in SCOP++, called "LiDAR DTM default" was applied to all last echoes in order to generate a DTM grid of 0.5m x 0.5m. A void filling step with a sampling interval of 3 m was applied on the resulting ground points of the first filtering, which is done to fill the holes where buildings and other high objects were eliminated. The "filled" dataset was then again interpolated using moving planes to obtain a final continuous terrain model with a resolution of 0.5 m. The result can be seen in figure 23. There are some holes and no continuous representing of the ground in some areas, which could be removed only by extensive manual editing.

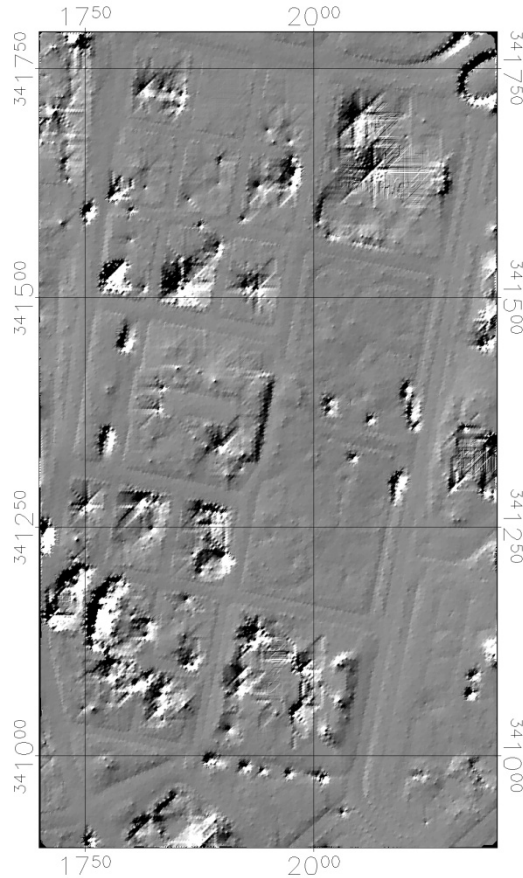


Figure 23. Shaded DTM of the test area.

- **DSM generation:**

For DSM generation we used a method as presented in [21] which is a combined approach of DSM_{max} , which is determined by the highest point within a defined raster cell, and DSM_{mls} , which is determined by heights derived through moving least squares interpolation e.g. moving planes. The DSM_{mls} is used for smooth surfaces (e.g. street and roof) and the DSM_{max} for rough surfaces (e.g. the high vegetation areas). The final surface model is defined as a function $f(x,y)$ of the layers (i.e. different data properties) and the two before mentioned surface models. $f(x,y)$ has to be within the minimum-maximum range of different models. The surface roughness σ_z proved to be a good property because it discriminate between street, house roofs and open areas on one hand, and strongly vegetated and rocky surfaces on the other hand [20]. To derive the land-cover dependent DSM (Figure 24), the modules `opalsCell`, `opalsGrid` and `opalsAlgebra` are used. For our work we used a cell size of 0.5 m to derive the DSM raster containing the maximum elevation of first echo points within the cell, thus obtaining DSM_{max} . We used moving planes with grid size of 0.5 m and nearest neighbors of 10 first echo points to derive DSM_{mls} . `OpalsAgebra` is employed to derive a grid or raster model by combining multiple input grid and/or raster data sets. We used it to combine the DSM_{max} and DSM_{mls}

depending on the σ_z layer (which is calculated as feature using opalsGrid). The heights of final DSM are calculated by this formula:

If ($Z[\sigma_z] < 0.2$) or ($Z[DSM_{max}] = \text{No Data}$)

Then $Z[DSM_{mls}]$

Else $Z[DSM_{max}]$

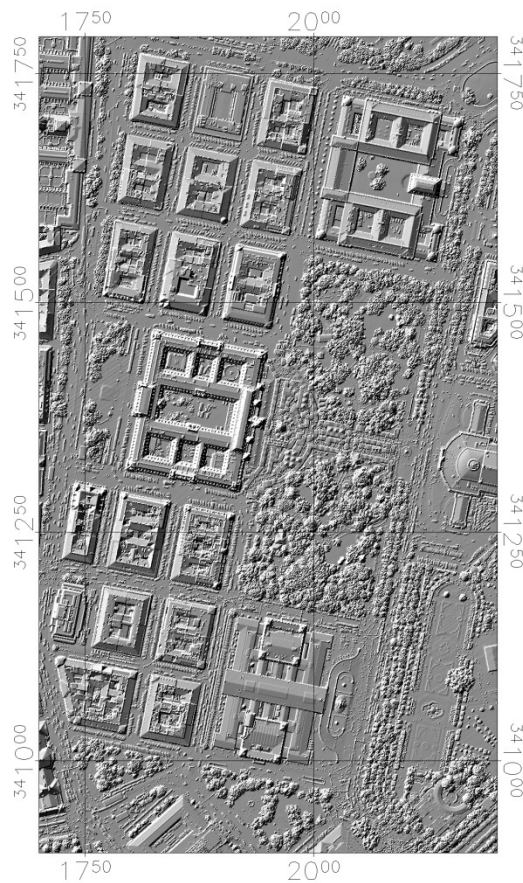


Figure 24. Shaded DSM of the test area.

- **nDSM generation:**

For derivation of nDSM opalsDiff module is used to derive difference grid models based on either two input grids or a single input grid and a horizontal reference plane. The generated DTM is subtracted from land-cover dependent DSM to obtain the nDSM (Figure 25).

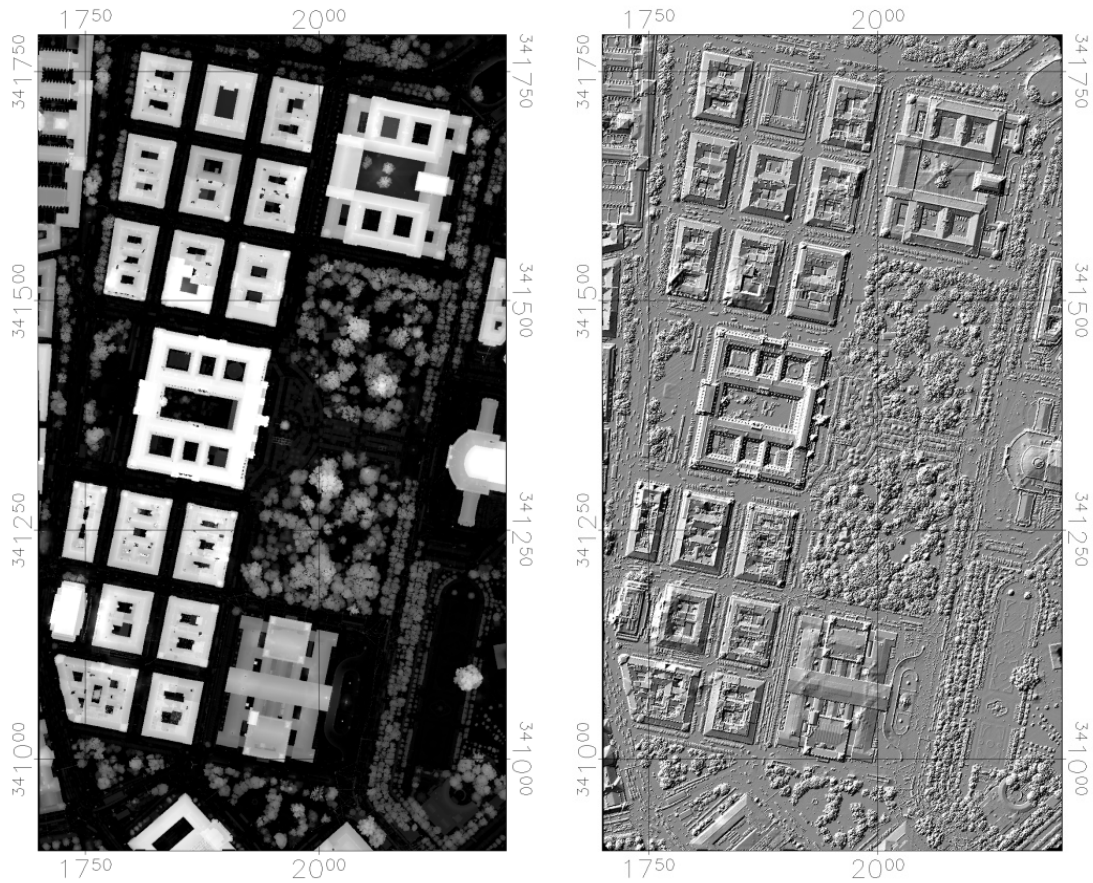


Figure 25. Left: nDSM, right: shaded image of nDSM

6.3.1.2 Slope (S):

As mentioned above the primary aim of opalsGrid is the derivation of surface grid models.

Using moving planes interpolation for each cell with grid size of 0.5 m and of 10 nearest neighbors the slope's model is derived. Slope for each grid cell corresponds to the inclination of an interpolated plane which is determined from the height of the grid cell and its neighbors. Slope feature describes the steepest slope in % for each cell. As we see in Figure (27, left) the highest values of the slope feature are in vegetation regions (trees) and the building edges. That means that slope can be used to discriminate between vegetation and other objects.

6.3.1.3 Sigma-Z (σ_z):

The Sigma-z model is generated as slope model,. Sigma-z is a parameter which describes the standard deviation of Z-value of grid post interpolation adjustment (Figure 26). As mentioned in section 6.3.1.1. sigma-z (σ_z) describes the surface

roughness. In Figure (27, right) it can be seen that the high values are in vegetation areas (trees and shrubs) while it is lower in flat areas like roads and roofs.

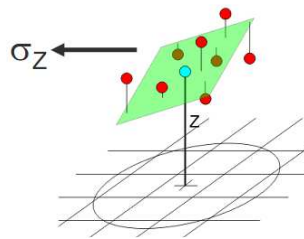


Figure 26. Sigma-z parameter

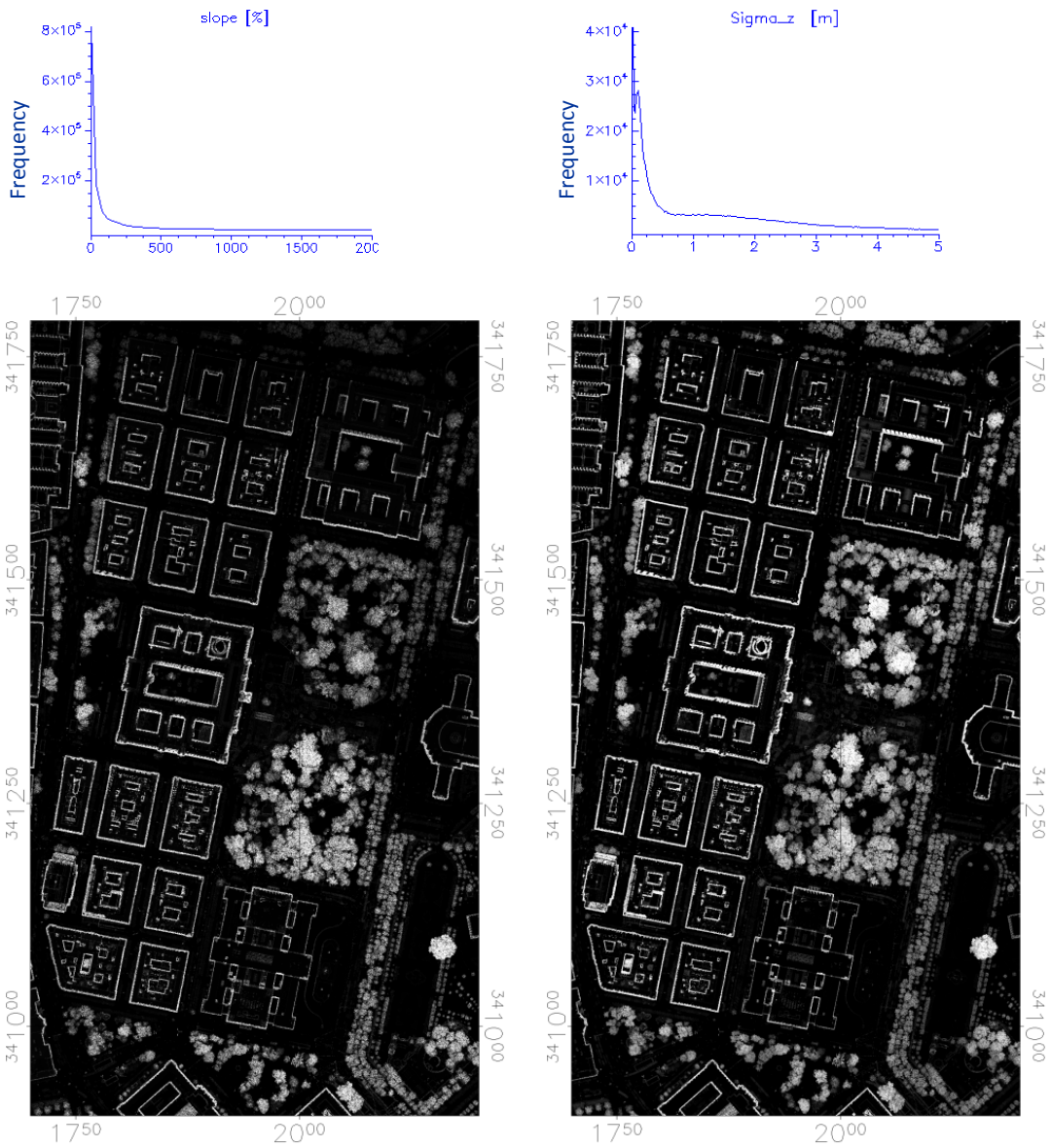


Figure 27. Left: Slope, S , right: Sigma-z, σ_z

6.3.2 Echo-based features

6.3.2.1 Number of echoes (Ne):

"Number of echoes" is one of the additional information obtained from FWF-ALS data and of many attributes, that are included in the ODM file (section 6.2). It is the total number of echoes within the waveform. It can be extracted using the opalsGrid module or opalsCell module with additional features like(min, max, mean, etc).

In our work we used opalsGrid module to derive feature's model of this attribute using grid size 0.5 m for all echo-points. From the histogram it is noticed that there are some values less than 1 due to the interpolation of the grid data and this value (one or less) is more for the open ground areas and roofs. We can see in Figure 28 the high values of this attribute are in vegetation areas (trees) and along the building edges.

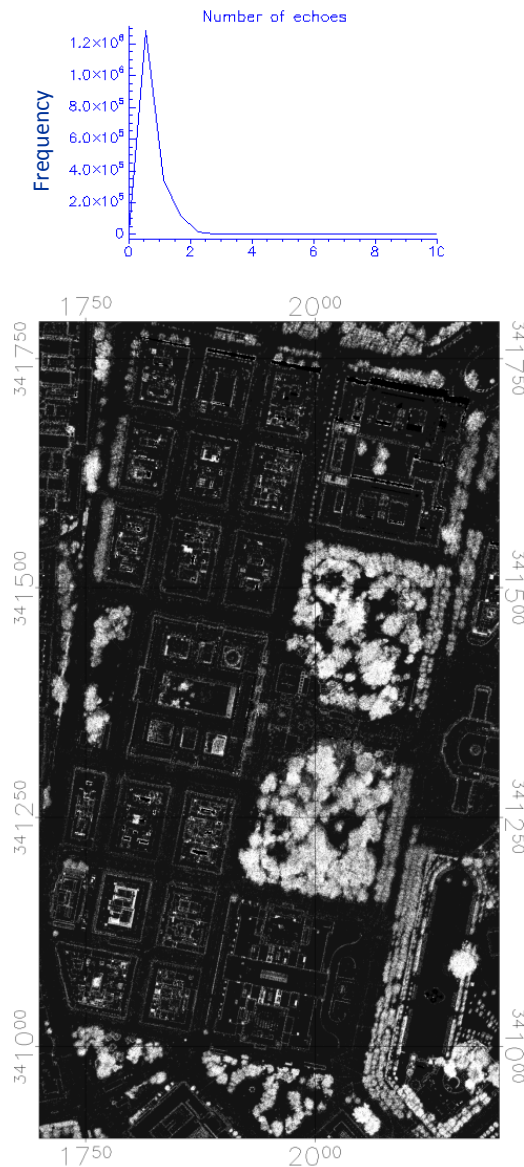


Figure 28. Number of echoes

6.3.3 Physical features:

6.3.3.1 Amplitude (A):

The maximum amplitude is a measure of the strength of the echo [1], and it is one of the additional information which can be extracted from full-waveform ALS data using Gaussian decomposition (section 2.3.1). Using opalsGrid or opalsCell module we can obtain the amplitude feature model and other additional features which describe different values of amplitude in each cell for all, first or last echoes. In our work we used opalsCell to derive a raster model of minimum and maximum attribute values of last echo points using cell size of 0.5 m (Figure 29).

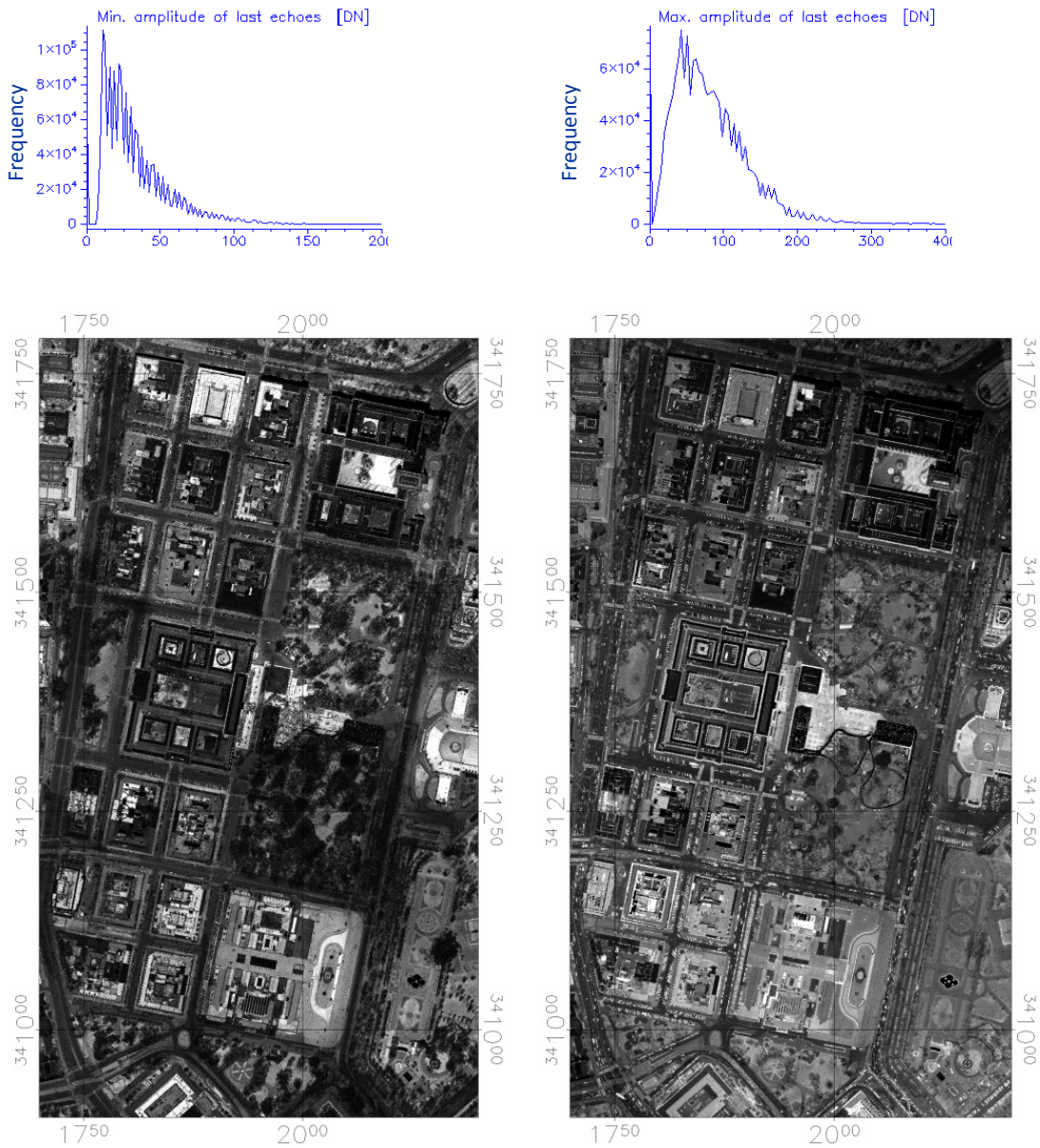


Figure 29. Left: Min. Amplitude of last echoes, right: Max. Amplitude of last echoes

6.3.3.2 Echo-Width (ew):

As discussed in section 2.3.1, another attribute which can be derived by Gaussian decomposition is echo-width. The echo-width could refer to the Full Width at Half the Maximum (FWHM) amplitude or the standard deviation of the echo in the Gaussian decomposition [1]. As shown in [25] and [13] the increased pulse width indicates large roughness of vegetation, slanted or small stepped surface. Vegetation spreads LiDAR pulses, therefore we found the highest width values in trees. Ground and building surfaces coincide with low width values. We used opalsCell to derive a raster model of maximum and minimum attribute values of last echo points using cell size of 0.5 m. In figure 30 the brightness of minimum values suggests great values for the echo width. Due to the low contrast the image has been heavily brightness and contrast enhanced for visualization. The actual values are, of course, smaller than those of the maximum echo width, what can be clearly seen in the histograms.

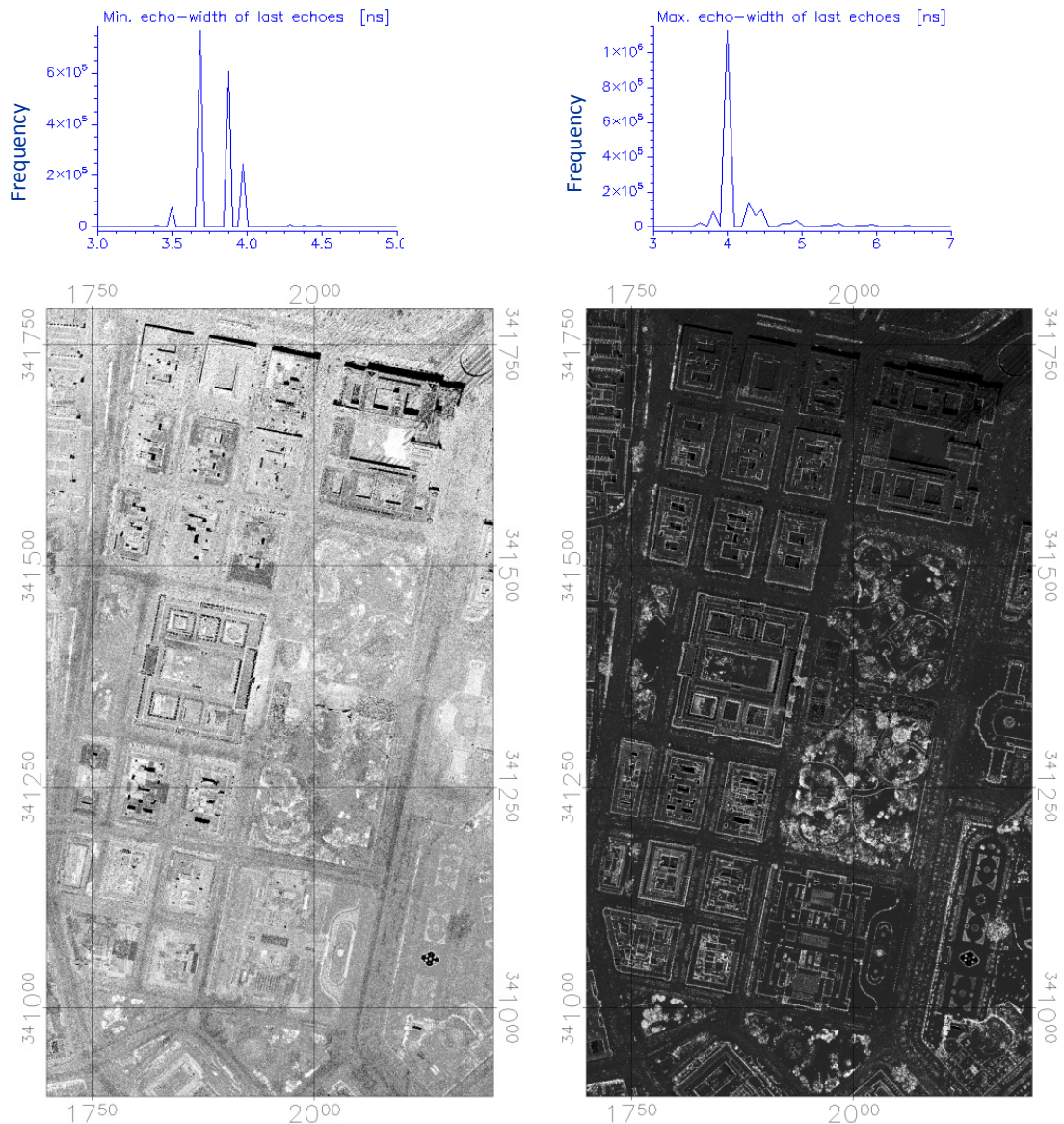


Figure 30. Left: Min. echo-width last echoes, right: Max. echo-width last echoes.

6.3.3.3 Backscatter coefficients γ and σ :

As mentioned in section 2.3.1, the additional information provided by the decomposition of full-waveform ALS data is suitable for calibration, whereby amplitude and echo-width are converted to values proportional to the surface reflectance of the target. In our work the FWF-ALS data is already calibrated using asphalt as reference surface and the backscattering coefficients γ and σ are estimated.

We used opalsGrid to derive these attributes, which the Cross-section σ [m^2] and Bi-static scattering coefficient γ [$\text{m}^2 \text{m}^{-2}$] are quantities for describing the scattering properties of the targets (Figure 31).

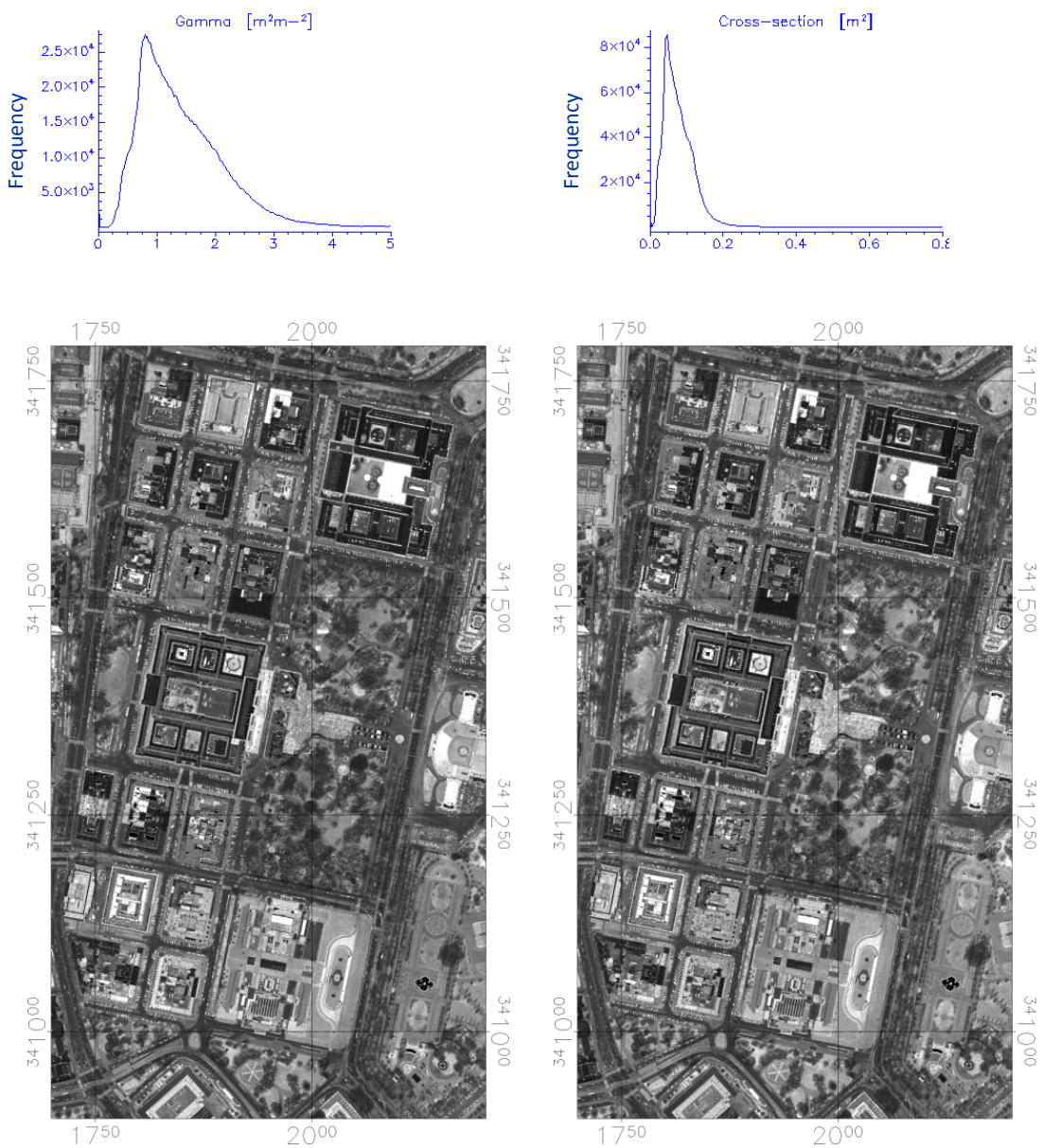


Figure 31. Left: Gamma (γ), right: Cross-section (σ).

7 Feature selection and classification accuracy

The objective of feature selection is to identify small sets of LiDAR features that can still achieve a good predictive performance. Thus correlated features should not be selected.

To select the most relevant features, we choose the following simple processing:

- Determining training areas and their analysis
- Applying classification (Maximum-Likelihood only) on test area iteratively, and at each iteration one or more of the features is excluded.

7.1 Determining training areas and their analysis:

Before the classification can be carried out, training areas must be determined for each class. Appropriate training areas are the base for good discrimination between classes. With help of an orthophoto of the study area the training areas are selected, where the data are homogeneous for each class (buildings, trees, roads, and grass areas) and in each LiDAR attributes.

The aim of this analysis is to determine appropriate characteristics for a clear discrimination between classes.

The analysis of the training data is based on frequency histograms, which display the distribution of the attributes (features).

As Figure (32-a) shows, that nDSM feature is a valuable one to discriminate between high objects in urban area, like buildings and trees, and low objects and/or ground areas.

As we see in Figure (32-b) the highest values of slope feature are in trees areas. That means, that slope can be appropriate to distinguish trees class from other classes.

Sigma-z describes the roughness of illuminated surface. We see in Figure (32-c), that sigma-z varies in the tree class from 0 to 6 m as maximum, while the maximum value for other classes is 1. That leads to the possibility of differentiating between trees and other classes using sigma-z, but one may find some high values of sigma-z for building class due to building edges.

As expected, Figure (32-d) shows that the highest value of number of echoes is in trees areas. As mentioned in section 6.3.2, some high values caused by building edges, in the histogram is showed too. That means, that this feature is useful to discriminate between trees class and other classes.

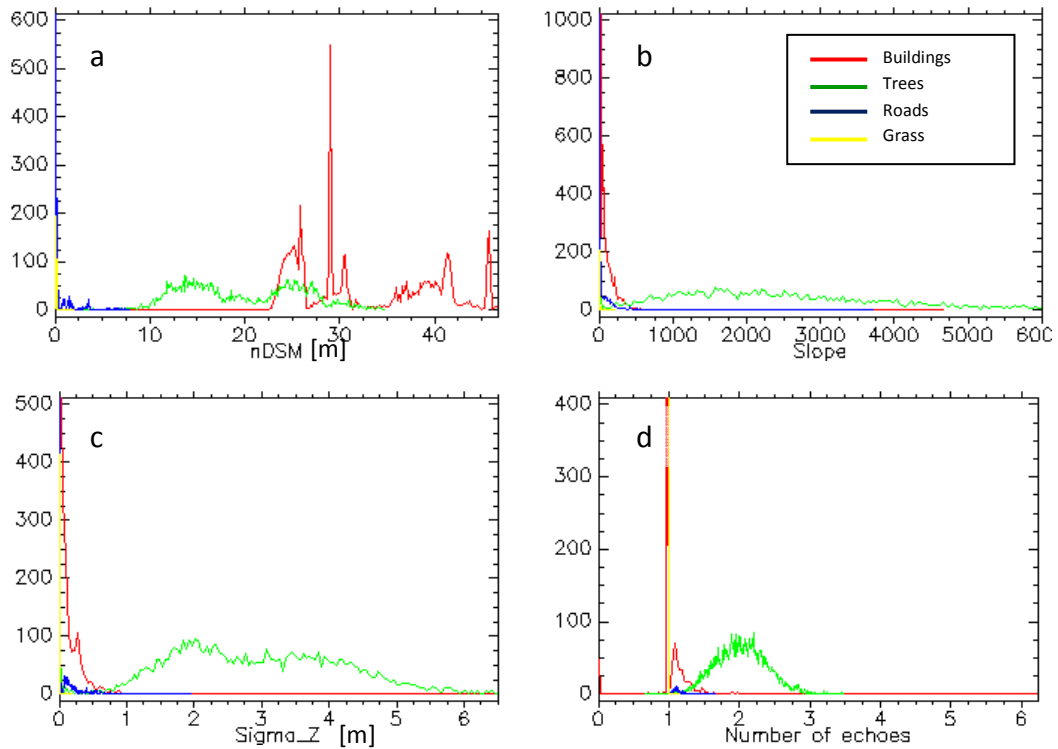


Figure 32. a) Normalized surface model (nDSM), b) Slope (S), c) Sigma-z (σ_z), d) Number of echoes (Ne).

As we can see in Figure 33, it is clear that with minimum and maximum amplitude of last echoes roads and grass areas can be discriminated. But it is difficult to be differentiated between roads and trees areas because of overlapping distribution as histograms show. Figure 34 show the 2D scattergrams each class. As we can see, the values of minimum amplitude for the building class varies more in the lower ranges of the maximum amplitude. The higher the maximum amplitude the higher the correlation to the minimum amplitude. For the trees class the minimal amplitude scatters more for low values of maximum amplitude than for high values. Roads show a similar behavior, but the minimum amplitudes are significantly smaller. The grass class scatters equally in two directions, and shows an ideal behavior of uncorrelation.

It is difficult to determine clear borders between classes for minimum and maximum echo width. We can say that the high values are more in trees areas (Figure 35).

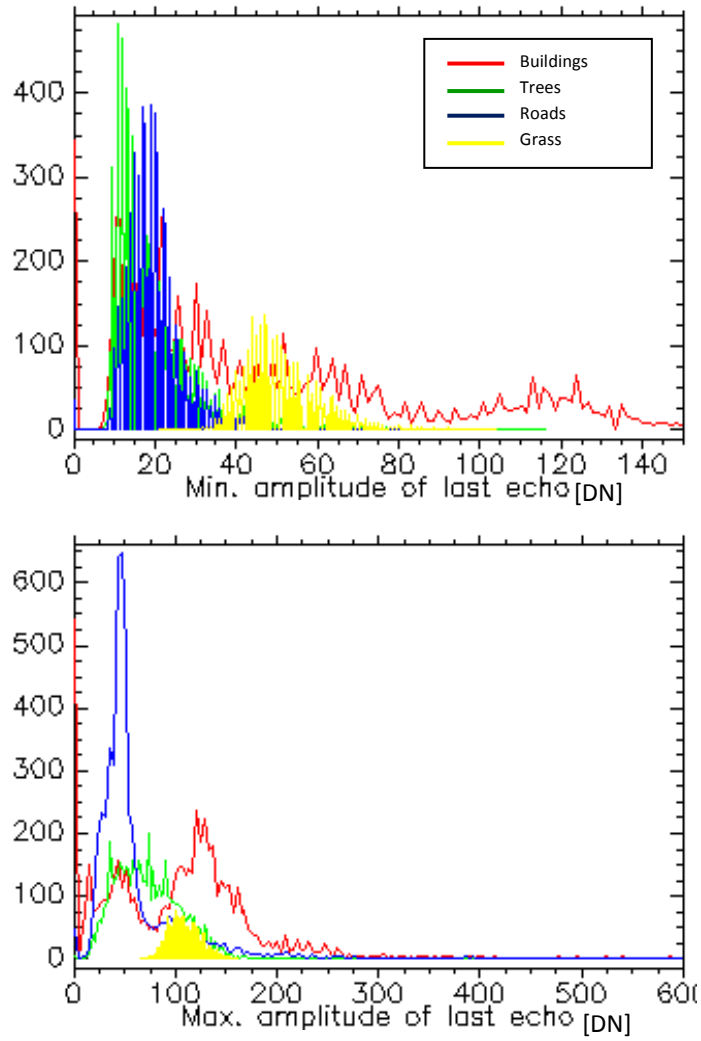


Figure 33. Above: Minimum amplitude, below: Maximum amplitude.

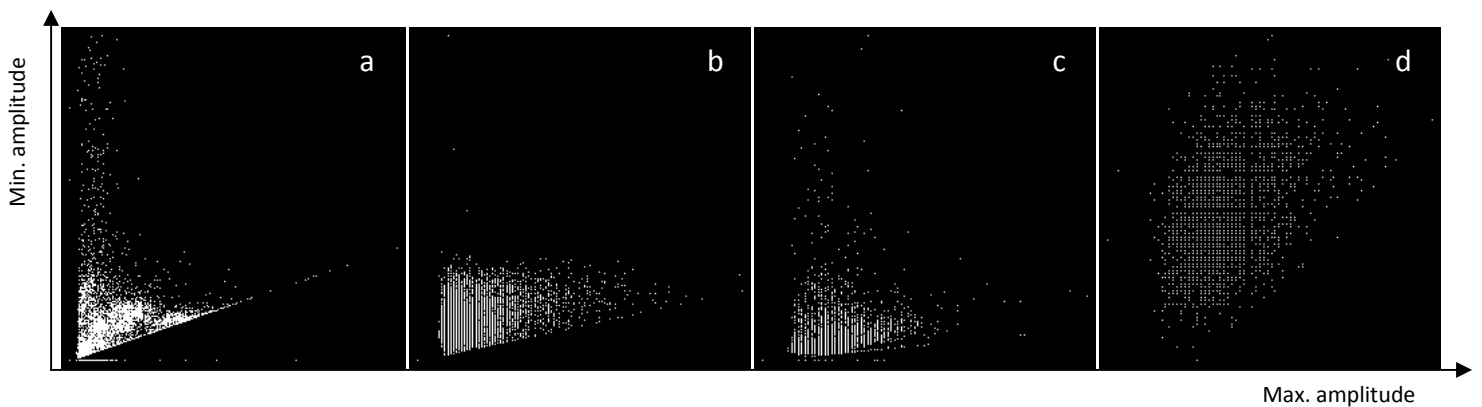


Figure 34. 2D plots (scattergram) each class for minimum amplitude and maximum amplitude features. a) buildings, b) trees, c) roads, d) grass class.

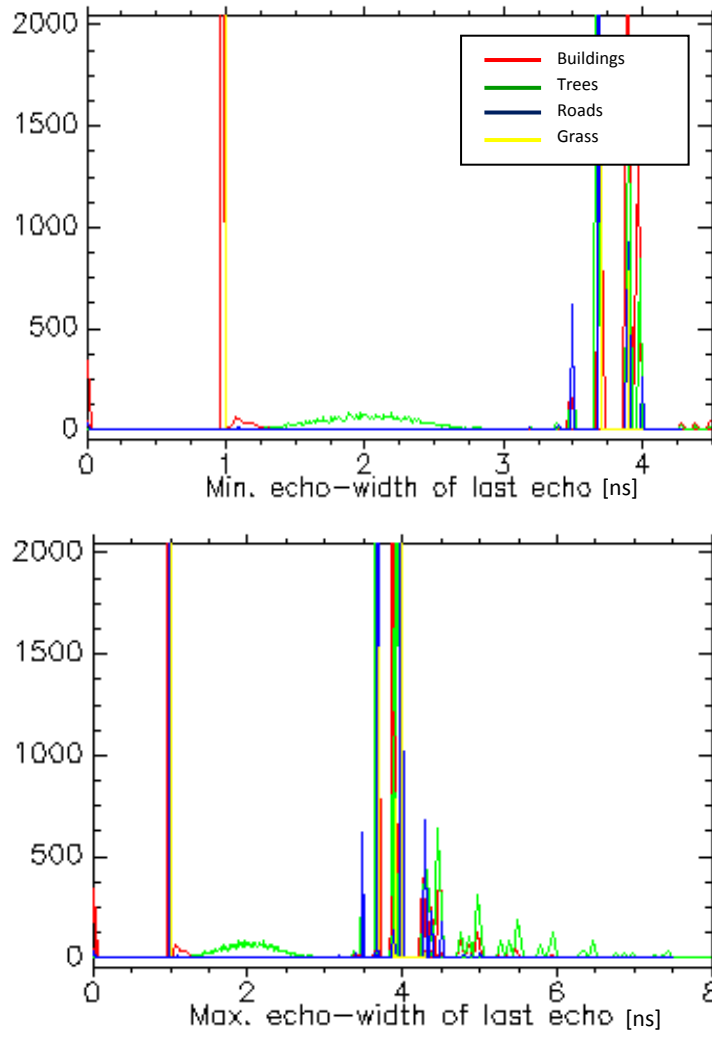


Figure 35. Above: Minimum echo-width, below: Maximum echo-width.

As Figure 36 shows, cross-section σ and gamma γ features are appropriate for distinguishing grass class from trees and roads classes.

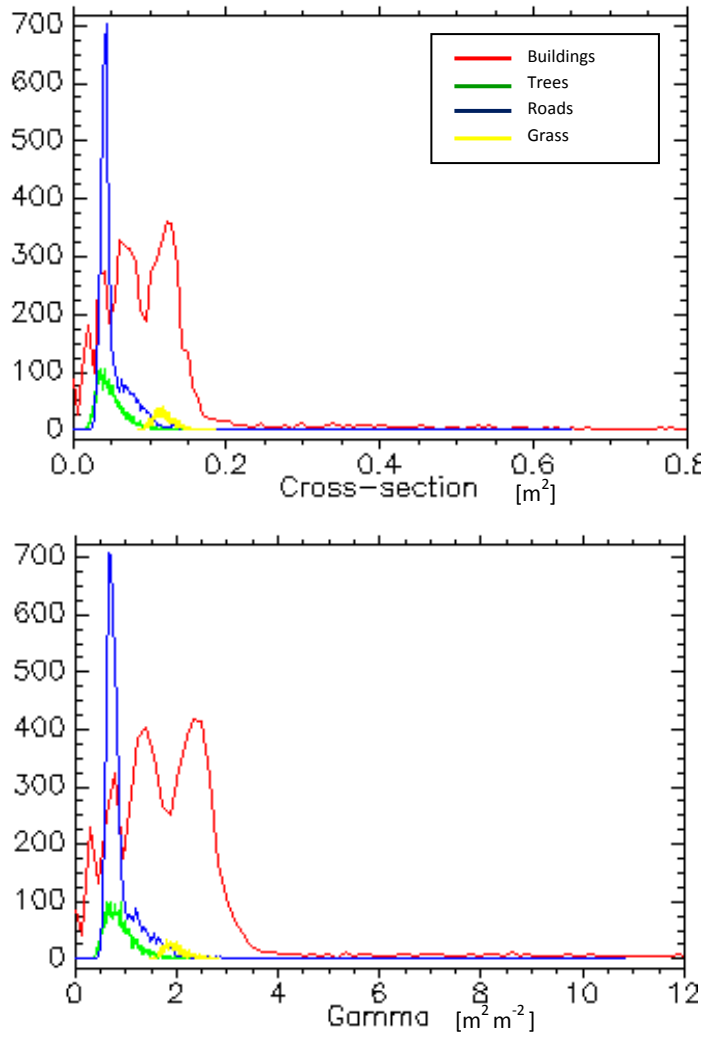


Figure 36. Above: Cross-section (σ), below: Gamma (γ).

- **Correlation between features (bands):**

Correlation matrix (Table 2) shows that there is, as expected, a high correlation between gamma and cross-section features (>0.9), and between minimum and maximum echo-width of last echoes features (0.76). But there is a low correlation between other features, varying between 0 and 0.6.

Features	S	σ_z	Ne	nDSM	Min. ew	Max. ew	γ	σ	Min. A	Max. A
S	1.000000	0.654671	0.394003	0.245918	0.016294	0.227172	-0.042782	-0.040894	-0.162977	0.091806
σ_z	0.654671	1.000000	0.429781	0.225547	-0.054608	0.095582	-0.049800	-0.047711	-0.146985	0.033361
Ne	0.394003	0.429781	1.000000	0.078579	0.086537	0.193593	-0.103408	-0.101115	-0.149350	-0.003409
nDSM	0.245918	0.225547	0.078579	1.000000	-0.013384	0.077115	0.043210	-0.010406	0.008240	0.082380
Min. ew	0.016294	-0.054608	0.086537	-0.013384	1.000000	0.763648	0.050516	0.050179	0.290674	0.226630
Max. ew	0.227172	0.095582	0.193593	0.077115	0.763648	1.000000	0.025921	0.024984	0.062973	0.241771
γ	-0.042782	-0.049800	-0.103408	0.043210	0.050516	0.025921	1.000000	0.988409	0.404378	0.382090
σ	-0.040894	-0.047711	-0.101115	-0.010406	0.050179	0.024984	0.988409	1.000000	0.396399	0.376220
Min. A	-0.162977	-0.146985	-0.149350	0.008240	0.290674	0.062973	0.404378	0.396399	1.000000	0.344548
Max. A	0.091806	0.033361	-0.003409	0.082380	0.226630	0.241771	0.382090	0.376220	0.344548	1.000000

Table 2. Correlation between all extracted features.

7.2 Classification and accuracy assessment:

One of the most common means of expressing classification accuracy is the preparation of a classification error matrix (or confusion matrix). Error matrices compare the relationship between known reference data (ground truth) and the corresponding results of an automated classification. The columns normally represent the reference data, while the rows indicate the classification generated from the remotely sensed data (in our case LiDAR data).

Overall accuracy is computed by dividing the total correct (sum of the major diagonal) by the total number of pixels in the error matrix.

$$\text{Overall accuracy} = \frac{\sum \text{correctly classified pixels}}{\sum \text{all pixels}}$$

Producer's accuracy is computed by dividing the total number of correct pixels in a class by the total number of pixels of that class as derived from the reference data (i.e. the column total). This statistic indicates the probability of a reference pixel being correctly classified and is measure of omission error.

$$\text{Producer's accuracy} = \frac{\sum \text{correctly classified pixels in a class}}{\sum \text{pixels in reference class}}$$

User's accuracy is computed by dividing the number of correctly classified pixels in each class by the total number of pixels that were classified in that class (i.e. the row total). The result is a measure of commission error. This statistic indicates the probability that a pixel classified on the map actually represents that class on the ground.

$$\text{User's accuracy} = \frac{\sum \text{correctly classified pixels in a class}}{\sum \text{pixels in a classified class}}$$

Kappa coefficient k is a measure of the difference between the actual agreement between reference data and an automated classifier and the chance agreement between the reference data and a random classifier.

$$k = \frac{\text{observed accuracy} - \text{chance agreement}}{1 - \text{chance agreement}}$$

This statistic serves as an indicator of the extent to which percentage correct values of an error matrix are due to "true" agreement versus "chance" agreement [32]. k is calculated with the help of the following formula:

$$k = \frac{N \sum_{i=1}^r x_{ii} - \sum_{i=1}^r (x_{i+} \cdot x_{+i})}{N^2 - \sum_{i=1}^r (x_{i+} \cdot x_{+i})}$$

Where:

- r = number of rows in the error matrix
- x_{ii} = number of observations in row i and column i (on the major diagonal)
- x_{i+} = total of observations in row i
- x_{+i} = total of observations in column i
- N = total of observations included in matrix.

- **Maximum-Likelihood classification:**

Applying Maximum-Likelihood classification algorithm iteratively, using the same training areas for each iteration, helps to determine the most appropriate feature. In each iteration one or more features will be excluded. The highest overall accuracy will determine the most relevant selected feature sets.

Because we don't have a large number of features (only 10 features), the iterative exclusion of LiDAR features will be done manually. The total number of sampled pixels, which are used as a ground truth, for each class are in Table 3.

Buildings	10883 pixels
Trees	6767 pixels
Roads	9673 pixels
Grass	3591 pixels
Total	30914 pixels
Image	1782781 pixels
Percent	1.73 %

Table 3. Sampled pixels as ground truth for accuracy assessment in test area.

To reduce the number of selected features, the high correlated features will be excluded. Therefore, gamma (which is highly correlated with σ) and maximum echo width of last echoes (which is highly correlated with the minimum echo width) will not be used. The minimum value of amplitude is more useful than the maximum amplitude to discriminate between road and grass classes, therefore we will use only minimum amplitude. As for cross-section, as seen from Figure 36 it seems to be slightly more useful than γ to distinguish between road and grass classes. Theoretically also γ should deliver good results. Because of the normalization to the Laser footprint, γ might be more appropriate in areas of great elevation differences. Further investigations should be carried out in those areas.

Therefore the features were reduced to the seven most relevant (Table 4).

Features	
Normalized digital surface model	nDSM
Slope	S
Sigma-z	σ_z
Min. amplitude of last echoes	Min. A
Min. echo-width of last echoes	Min. ew
Number of echoes	Ne
Cross-section	σ

Table 4. Used features in classification.

• **Observations:**

Figure 37 illustrates the overall accuracy of iterative classification applied to different combinations of selected features. Figure 38 illustrates the producer's accuracy for each class.

We observe that some combinations seem to be better than the others with respect to overall and producer's accuracy.

1. Using just the geometric features, i.e. nDSM, slope, and sigma-z, yields the lowest overall accuracy (67.30 %). But we find that it is quite effective for detecting buildings, trees and grass classes (producer's accuracy > 80 %). For road class the classification is the worst (producer's accuracy < 20 %). This may be explained by the lack of the use of FWF-ALS features (min. A, min. ew, σ , Ne), because, as mentioned before, these features describe the physical properties of different materials in the observed scene. Figure (39-b) shows the classification result using this combination.
2. Excluding only nDSM feature doesn't increase the overall accuracy (67.40 %). As for producer's accuracy results for buildings is very poor(<40 %), while for roads significantly better results could be achieved. This effect is understandable because the height (nDSM) did not play a role and therefore many parts of buildings are counted as roads thus apparently improving the quality of the classification of roads. This emphasizes the important role of the nDSM in urban classification. The classification of trees and grass has slightly improved, but this might be a side effect of not including nDSM if the entire series of classifications in compared in Figure 38.
3. Excluding physical features, i.e. cross-section, min. amplitude and min. echo-width, slightly improved the overall accuracy (69.74 %), while the accuracy for roads decreased (20.23 %). That means these features are valuable features for roads discrimination.
4. Comparing with (3) there is almost no change, overall and producer's accuracy remain the same, if minimum amplitude and minimum echo width are included.

5. By including the cross-section can be seen that the classification significantly improved (84.92 %), although minimum amplitude of last echoes feature has not been taken into account. This significant improvement for the road classification can be observed in all other classifications where the cross-section was included.
6. No significant change in classification results by using all features compared to (5), maybe there is a slight improvement for the road class caused by minimum amplitude. A similar effect can be observed from (3) to (4), and later from (8) to (9).
7. Excluding number of echoes doesn't change the overall accuracy of the classification, but it can be seen that it negatively influences the result for the tree class. The number of echoes is a characteristic feature for vegetation and therefore this result is understandable. The slight improvement for road class might again be a side effect. Some trees along roads are not detected as trees anymore and are added to the road class.
8. No significant change in the classification results by excluding both min. amplitude and min. echo-width or
9. By excluding min. echo-width only.
- 10.. Excluding only sigma-z (σ_z) doesn't change the overall accuracy. Compared to (8) this combination slightly improves the road class and in a similar way decreases the accuracy of the buildings. Again this opposite behavior could be a side effect, when building edges with their high sigma-z values are partly counted as roads.
11. Compared to (10) excluding the slope by keeping all other features seems to improve the classification of buildings. By comparing the accuracy of building the previous classification (except (2)) no improvement can be observed. The importance of slope for the classification, as it is investigated in this work, is, therefore, questionable.
12. Compared to all other combinations, excluding both slope (S) and sigma-z (σ_z) improves the overall accuracy and yields the highest value (89.34 %). Again it can be observed that an improvement for the road class is accompanied by a deterioration of the building class. Figure (39-c) shows the classification result of this combination.

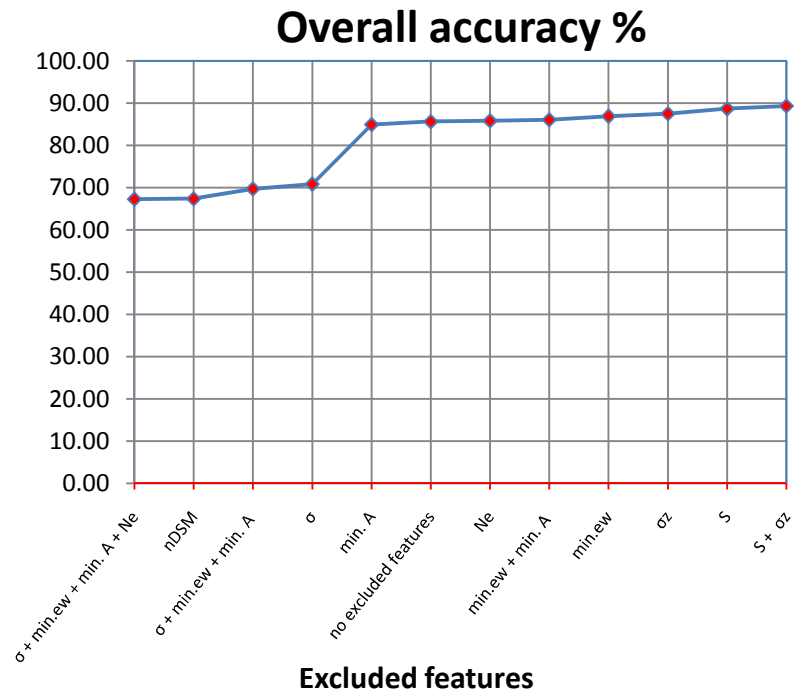


Figure 37. Overall accuracy of the iterative classifications using Maximum-

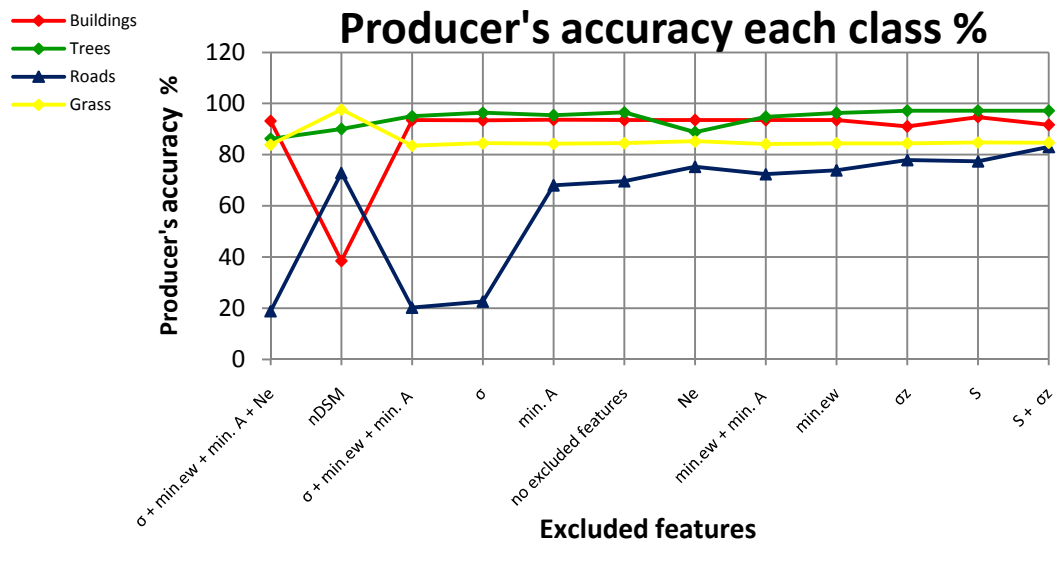


Figure 38. Producer's accuracy of each class of the iterative classifications using Maximum-likelihood.

We can briefly summarize few important observations for classification results by using FWF-ALS features and Maximum-Likelihood classifier in urban area:

- Height feature (nDSM) is the most important classifier for buildings (compare (6) and (2)).
- Number of echoes feature (N_e) plays an important role in classification of trees areas (compare (6) and (7)).
- Cross-section (σ) is useful for roads discrimination (compare (4) and (6)).
- Minimum amplitude (min. A) of last echoes is of less importance, although it may be responsible for a slight improvement for roads and trees (compare transitions from (5) to (6) and from (8) to (9)).
- Minimum echo width (min. ew) of last echoes is of less importance (compare (9) and (6)).
- Adding sigma-z improves the classification of buildings (compare (6) and (10))

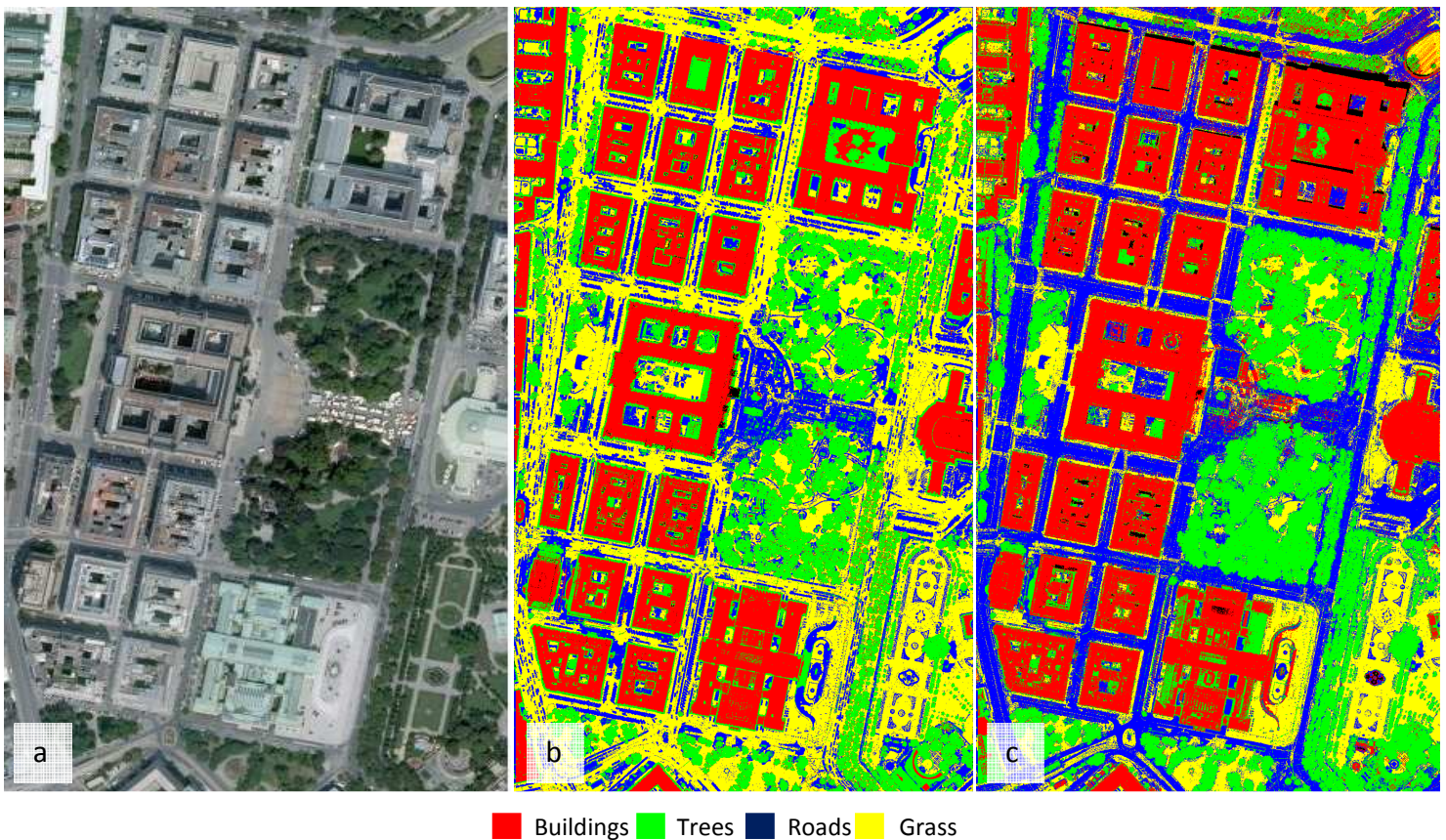


Figure 39. a) aerial image of test area, b) classification result using only slope, sigma-z and nDSM features, c) classification result excluding slope and sigma-z features. It is noted the improvement in the roads classification results using full-waveform ALS data.

- **Decision tree classification:**

Five simple decision trees generated using the training data analysis were used to classify the points. In the first decision tree all selected features are used, in the second one five features are used (without slope and sigma-z), for third tree minimum echo-width is not used, minimum amplitude feature is excluded in the fourth tree and in the fifth one cross-section (σ) is excluded. Table 5 shows the features excluded in each decision tree. The classification results using the five decision trees are compared and discussed.

Decision tree	Excluded feature
Tree 1	No exclusions (6)
Tree 2	S, σ_z (12)
Tree 3	min. ew (9)
Tree 4	min. A (5)
Tree 5	σ (4)

Table 5 . Generated decision trees

The basic structure of the decision trees remained the same. Just by removing individual feature (according to Table 5) some nodes may have been removed and therefore the five decision trees eventually have different numbers of nodes. The same sampled pixels, used as ground truth in Maximum-Likelihood classification (Table 3), were used in the classification accuracy assessment using these five decision trees. The threshold in for the rules (decision made in a node) have been visually derived from the histograms (compare Figures 32, 33, 35 and 36)

- The first decision tree (all features) has 13 nodes, five attributes (nDSM, Ne, S, σ_z , min.ew) were required to discriminate between buildings and high trees. Two attributes (nDSM, min.ew) were used to discriminate the small trees from roads and grass classes. Four attributes (nDSM, min.ew, min. A, σ) are required to classify roads and grass area. Figure 40 illustrates the first decision tree.
- The second tree has 11 nodes, slope and sigma-z attributes were excluded. Three attributes (nDSM, Ne, min.ew) were used to classify trees and buildings, and four attributes (nDSM, min.ew, min. A, σ) were used to discriminate between roads and grass see Figure 41.
- The third tree has 9 nodes, and minimum echo-width feature were excluded. Four attributes (nDSM, Ne, S, σ_z) were used for buildings and trees classification and three attributes (nDSM, min. A, σ) for roads and grass classification (Figure 42).
- The fourth tree based on minimum echo-width and cross-section attributes in the classification. It has 13 nodes, five attributes (nDSM, Ne, S, σ_z , min.ew) were required to discriminate between buildings and high trees. Two attributes (nDSM, min.ew) were used to discriminate the small trees from roads and grass classes.

Three attributes (nDSM, min.ew, σ) are required to classify roads and grass area (Figure 43).

- In the fifth tree the classification based on minimum amplitude and minimum echo-width as FWF attributes. It has 13 nodes, five attributes (nDSM, Ne, S, σ_z , min.ew) were required to discriminate between buildings and high trees. Two attributes (nDSM, min.ew) were used to discriminate the small trees from roads and grass classes. Three attributes (nDSM, min.ew, min. A) are required to classify roads and grass area (Figure 44).

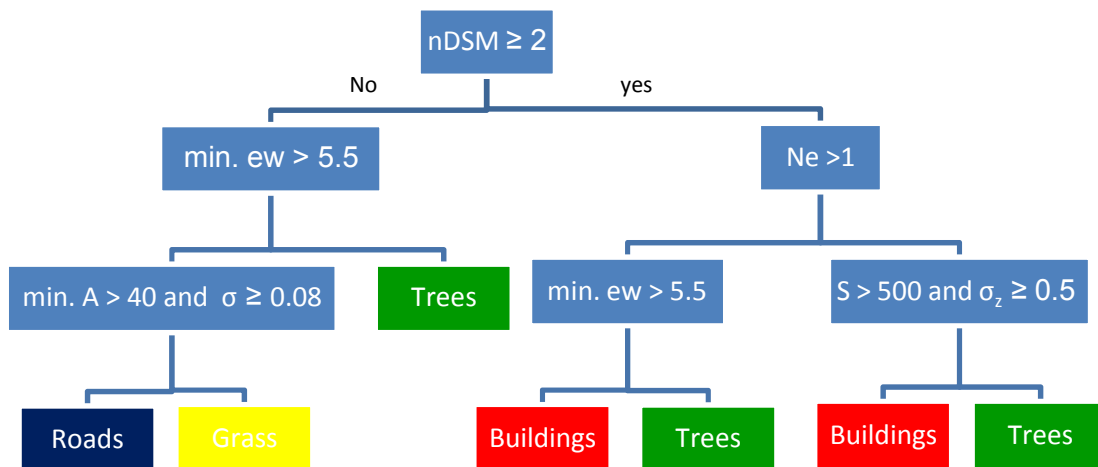


Figure 40. First decision tree used for the classification of test area.

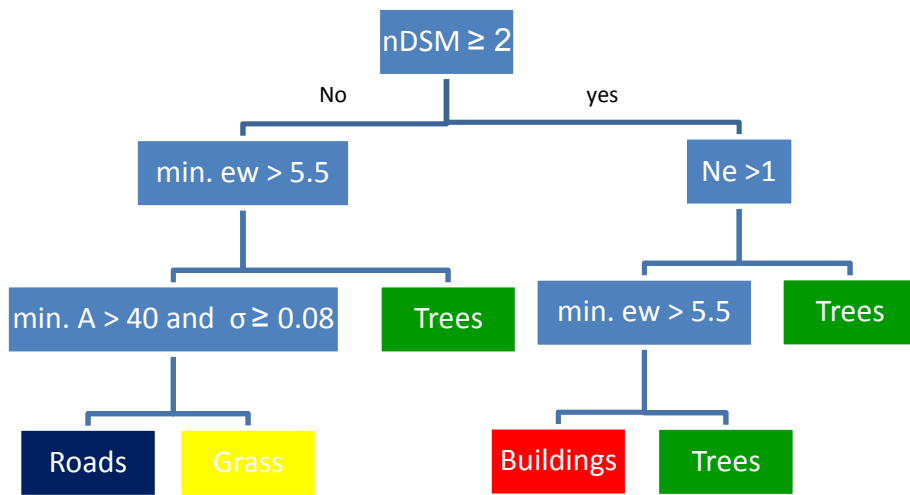


Figure 41. Second decision tree used for the classification of test area.

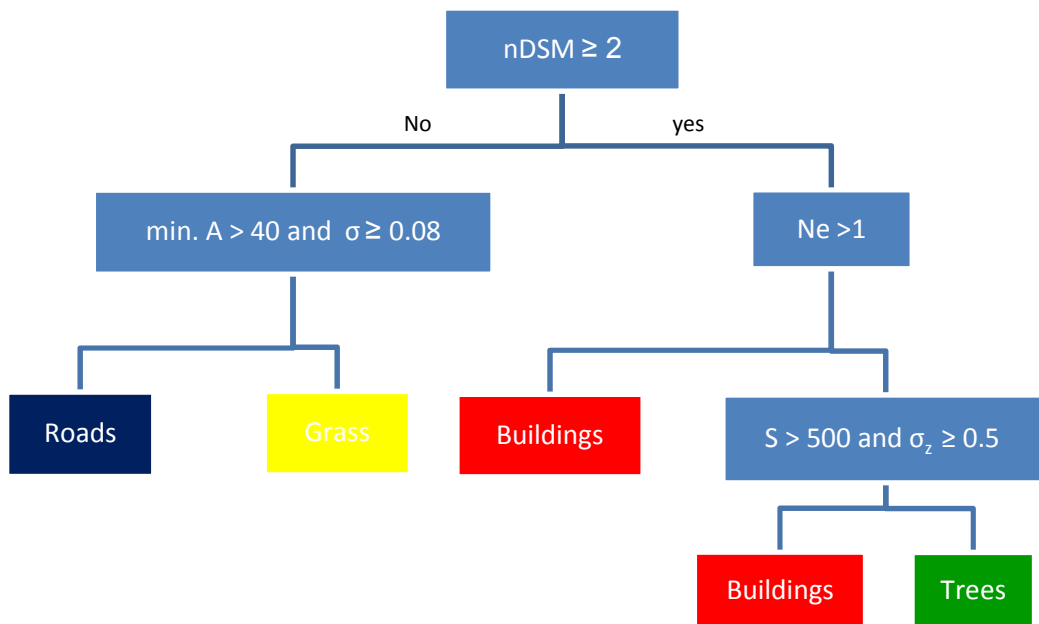


Figure 42. Third decision tree used for the classification of test area.

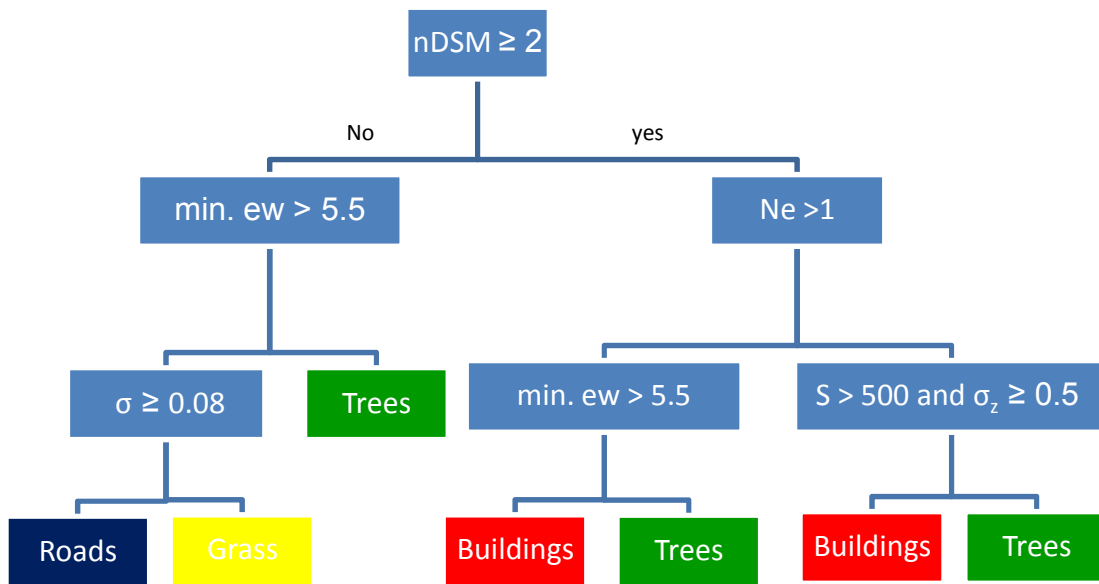


Figure 43. Fourth decision tree used for the classification of test area.

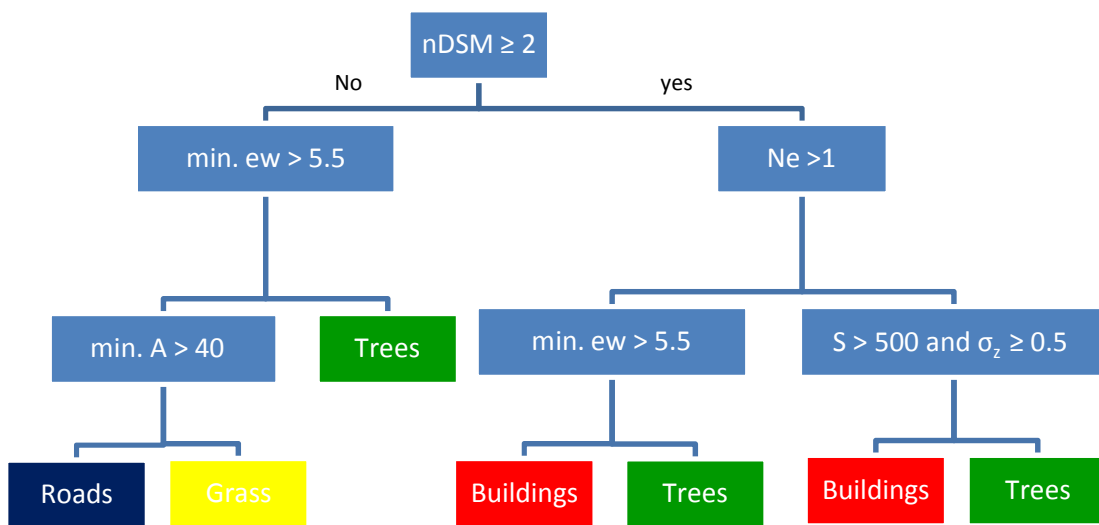


Figure 44. Fifth decision tree used for the classification of test area.

- **Results and classification accuracy:**

The average overall accuracies for all five decision trees classification is high (>80 %). It can be seen from Table 6, that the classification excluding slope (S) and sigma-z (σ_z) gave the lowest number of correctly classified building pixels (tree 2). In contrary this classification gave the highest producer's accuracy of trees (88.77 %). Excluding minimum amplitude gave the lowest number of correctly classified roads pixels (tree 4), while the average producer's accuracy of grass classification is 82 % for all decision trees. The classification excluding minimum echo-width feature (tree 3) gave the highest overall accuracy of 87.81 %.

The values representing the incorrectly classified pixels, which are more than 10 % of the total number, are red underlined in the Table 6. There are 2469 pixels that are classified as trees excluding slope (S) and sigma-z (σ_z) and 1869 (2469-600) correctly classified as buildings for other decision trees. 998 pixels are classified as buildings for decision trees 1, 3,4, and 5 , while 949 (998-49) correctly as trees in the classification excluding slope (S) and sigma-z (σ_z). By excluding minimum amplitude 1046 pixels are classified as grass. There are 507 pixels are classified as buildings for all decision trees.

Figure 45 shows the classification results of decision trees 2 and 4. It is clearly noted that excluding slope (S) and sigma-z (σ_z) is better for roads and trees classification, and the majority of buildings edges are classified as trees due to the number of echoes ($N_e > 1$).

Comparing with classification excluding min. amplitude, roads and grass require min. amplitude for their classification.

By excluding minimum amplitude the zebra strips are clearly appeared and classified as grass, and buildings are more clearly classified but there are some trees classified as buildings due to the overlap between slopes and sigma-z of buildings and trees in some areas. Nevertheless, some pixels classified as grass in all decision trees classification are classified incorrectly due their reflectance. Water has low reflectance in the infrared wavelength, leading to the inland water body being classified as road. Some of vehicles were classified as buildings due to their elevation from the ground (>2m).

Decision trees	Class	buildings	trees	roads	grass	Total	Producer's accuracy %	User's accuracy %	Overall accuracy %
Tree 1	buildings	10229	<u>998</u>	450	<u>507</u>	12184	93.99	83.95	87.79
	trees	600	5058	70	5	5733	74.75	88.23	
	roads	53	528	8895	121	9597	91.96	92.69	
	grass	1	183	258	2958	3400	82.37	87.00	
	Total	10883	6767	9673	3591	30914			
Tree 2	buildings	8360	49	376	<u>506</u>	9291	76.82	89.98	84.81
	trees	<u>2469</u>	6007	144	6	8626	88.77	69.64	
	roads	53	528	8895	121	9597	91.96	92.69	
	grass	1	183	258	2958	3400	82.37	87.00	
	Total	10883	6767	9673	3591	30914			
Tree 3	buildings	10230	998	450	<u>507</u>	12185	94.00	83.96	87.81
	trees	599	5058	70	5	5732	74.75	88.24	
	roads	53	524	8873	93	9543	91.73	92.98	
	grass	1	187	280	2986	3454	83.15	86.45	
	Total	10883	6767	9673	3591	30914			
Tree 4	buildings	10229	<u>998</u>	450	<u>507</u>	12184	93.99	83.95	85.63
	trees	600	5058	70	5	5733	74.75	88.23	
	roads	50	215	8107	0	8372	83.81	96.83	
	grass	4	496	<u>1046</u>	3079	4625	85.74	66.57	
	Total	10883	6767	9673	3591	30914			
Tree 5	buildings	10229	<u>998</u>	450	<u>507</u>	12184	93.99	83.95	87.27
	trees	600	5058	70	5	5733	74.75	88.23	
	roads	53	508	8734	121	9416	90.29	92.76	
	grass	1	203	419	2958	3581	82.37	82.60	
	Total	10883	6767	9673	3591	30914			

Table 6 . Error matrix for each decision tree, overall accuracy and producer's and user's accuracies for the classification of 5 trees are shown.

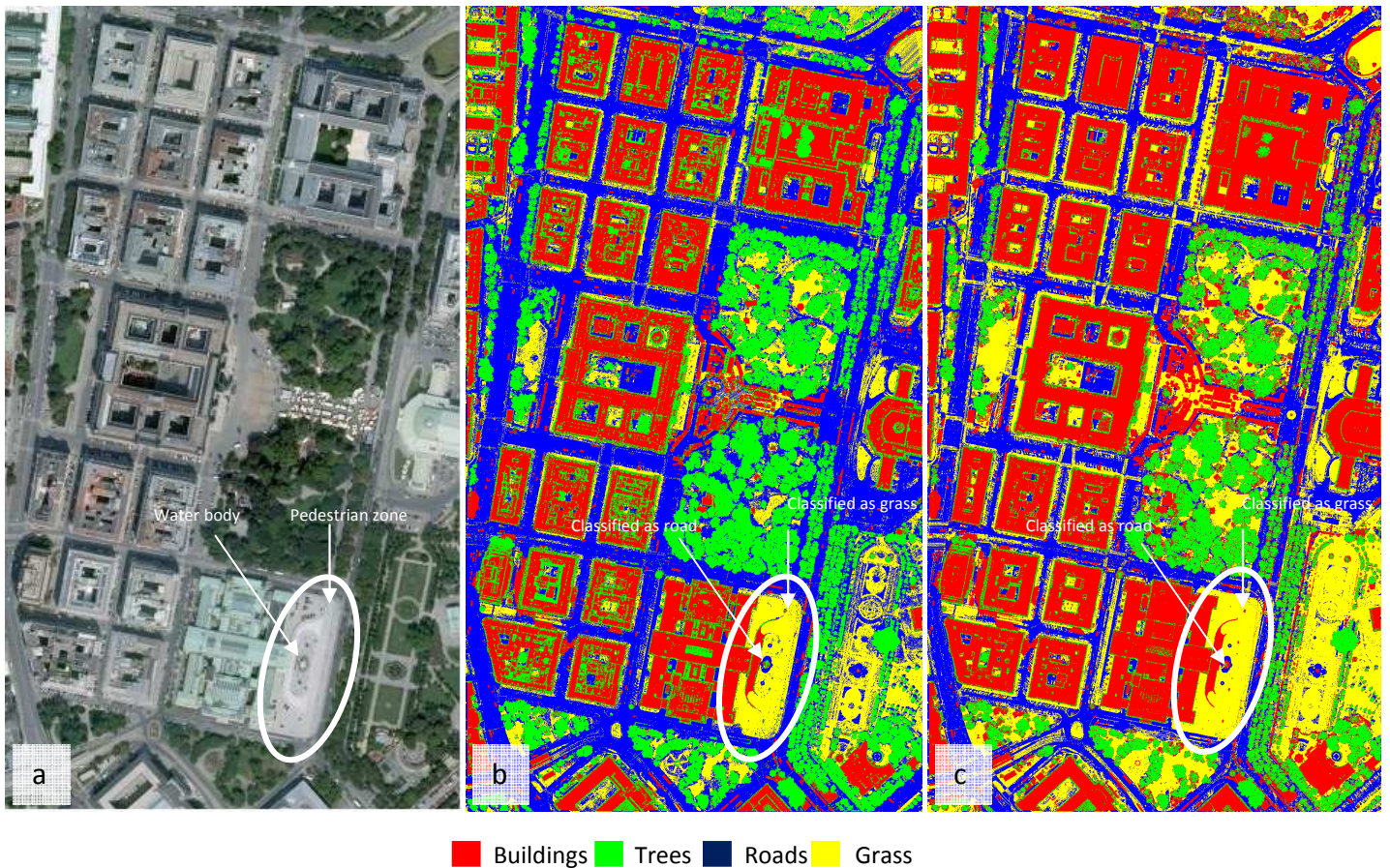


Figure 45. Classification results using decision trees, a) aerial image, b) excluding slope (S) and sigma- z (σ_z), c) excluding minimum amplitude.

• **Comparison between Maximum-Likelihood and Decision Tree classification:**

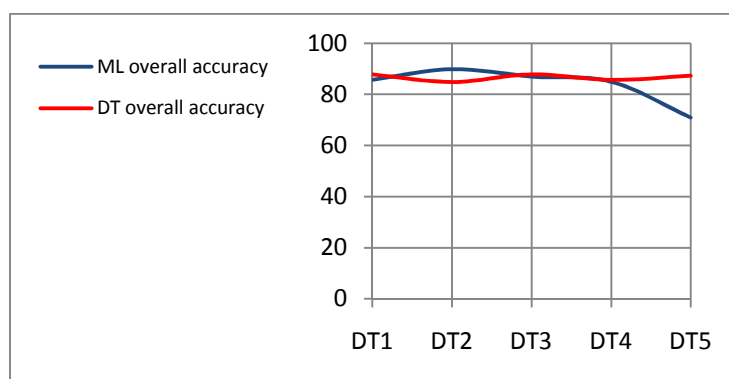


Figure 46. Comparison of overall accuracies of Maximum-Likelihood and Decision Tree classification for test area.

As comparison of Maximum-Likelihood and Decision Tree classification for some combinations, it is found that Decision Tree method gave better overall accuracy as we can see in Figure 46. The reason could be that Maximum-Likelihood depends on normal distribution in the features space, which it does not exist for features used

for the classification on one hand, on other hand Decision Tree depends on thresholds which can be determined exactly to discriminate between classes. Thus using Maximum-Likelihood, using these features, could not be an appropriate method for classification of urban areas.

8 Classification of the entire area

8.1 Maximum-Likelihood and Minimum-Distance classification:

After examining the test area, we will apply the classification on the entire study area using the same selected features extracted from FWF-laser scanning data (Table 4) except slope feature. Maximum-Likelihood and Minimum-Distance classifiers will be applied using the same training areas used for test area.

All features for the entire study area are extracted as mentioned in section 6.3. Two combinations of selected features are used for classification of all study area applying Maximum-Likelihood and Minimum-Distance. The first combination includes 6 features ($nDSM$, σ_z , $\min. A$, $\min. ew$, Ne , σ) corresponds to case (11) in section 7.2, the second one includes 5 features ($nDSM$, $\min. A$, $\min. ew$, Ne , σ) and corresponds to case (12).

Figures 47, 48, 49 and 50 show all the extracted features of entire study area with raster resolution of 0.5 m, independent of their use for classification..

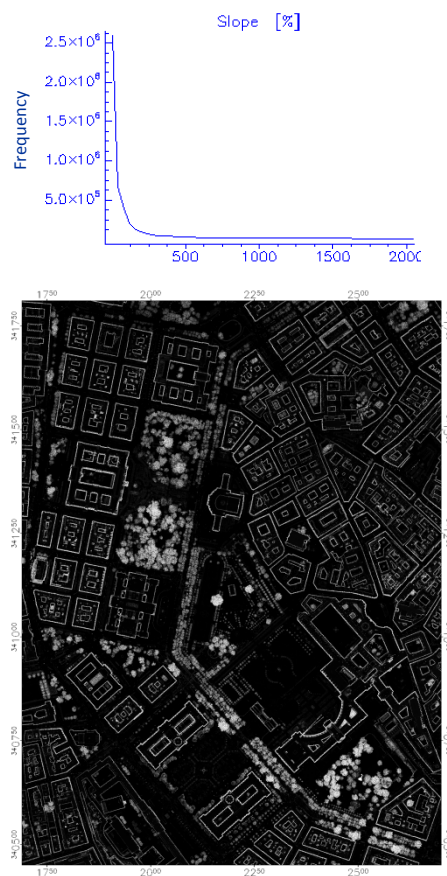


Figure 47. Slope (S)

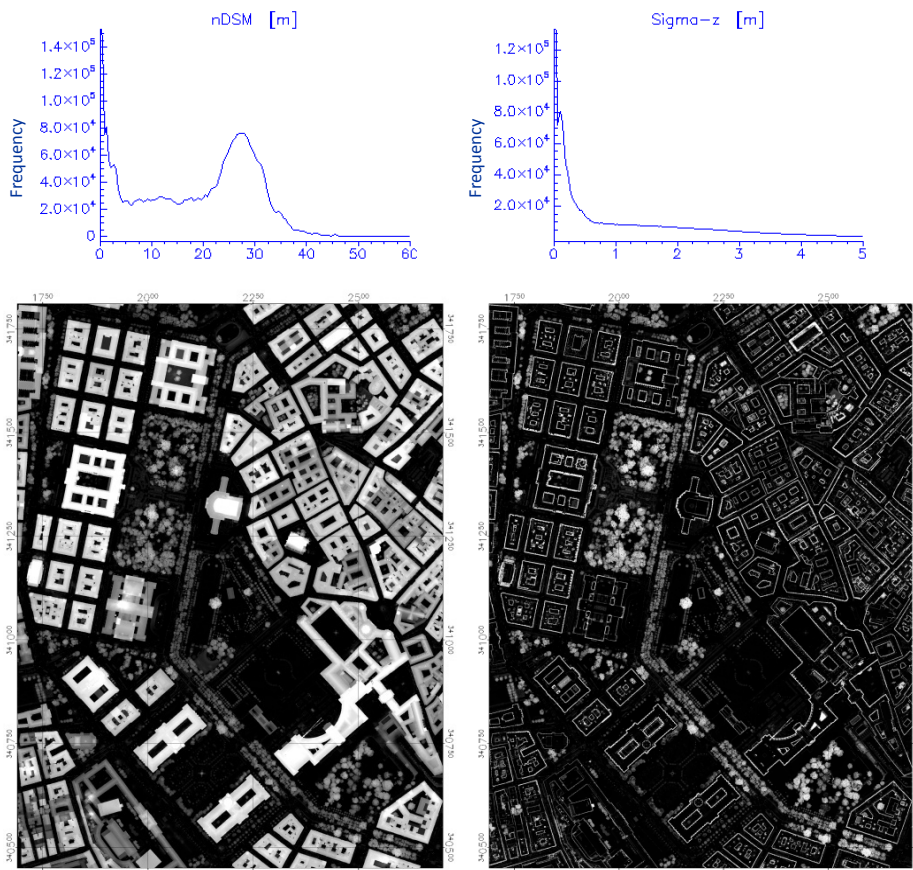


Figure 48. Left: nDSM, right: Sigma-z (σ_z).

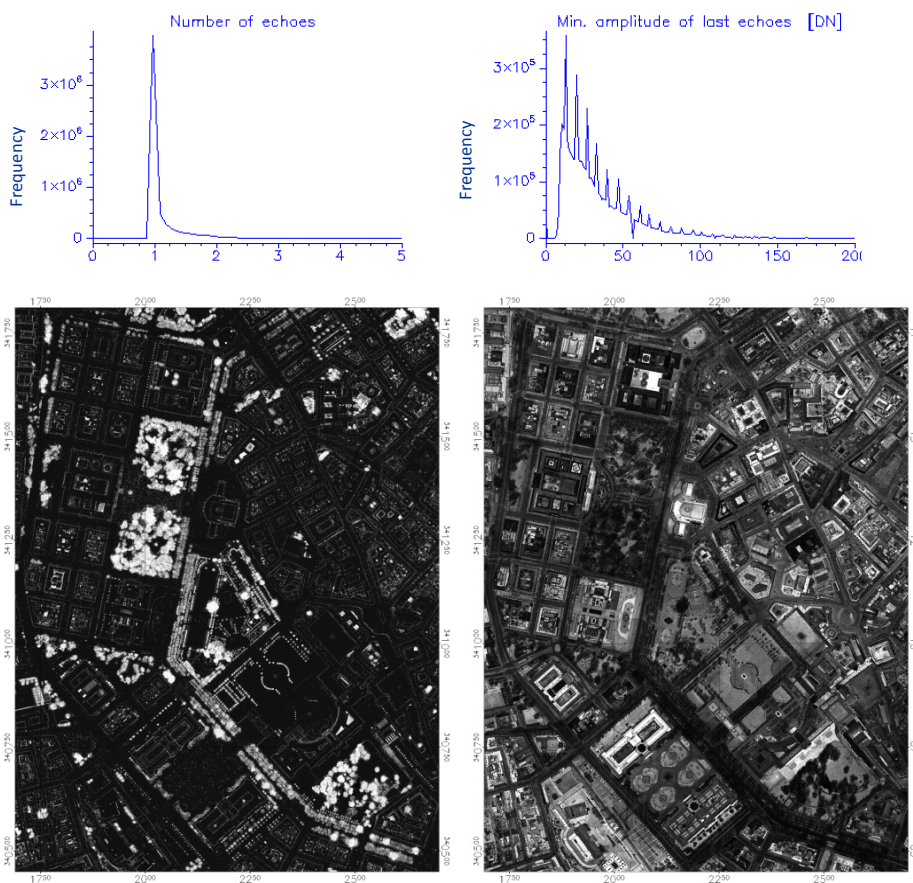


Figure 49. Left: Number of echoes (N_e), right: Min. amplitude (A).

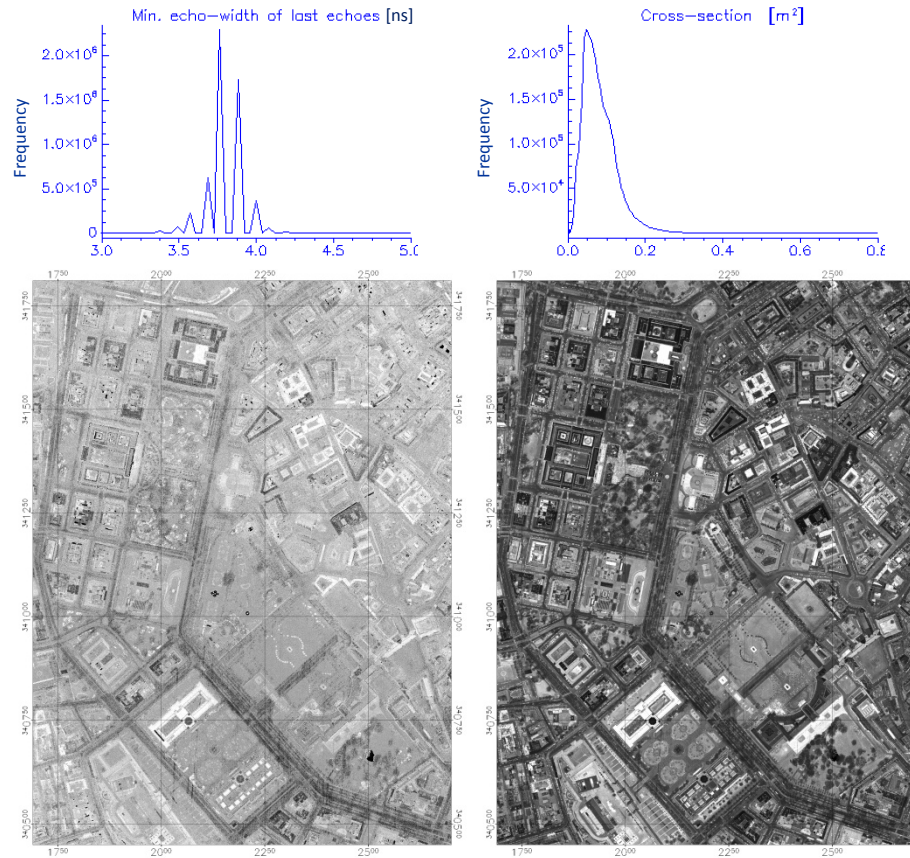


Figure 50. Left: Min. Echo-width (ew), right: Cross-section (σ).

8.2 Results and accuracy assessment:

Table 7 illustrates the classification results of Maximum-Likelihood and Minimum-Distance of the two combinations of extracted features for whole study area. As we can see, the overall accuracy of Maximum-Likelihood classification for both combinations is much better than Minimum-Distance one.

The classification with the first combination (excluding slope feature) yielded the overall accuracy of 77.10 % and a kappa coefficient of 0.69 for Maximum-Likelihood, and overall accuracy of 65.91 % and kappa coefficient of 0.55 for Minimum-Distance. The poor accuracy of the Minimum-Distance classification is caused by the poor accuracies of the classes buildings and trees, as it can be seen in the Table 7. The producer's accuracies of buildings and trees in Maximum-Likelihood classification are much better than those of Minimum-Distance. Roads are more correctly classified in Minimum-Distance. The results for grass are nearly the same for both classification methods.

In the second combination (excluding slope and sigma-z features), we can see some improvement in Minimum-Distance classification. This combination yielded for the Maximum-Likelihood classification an overall accuracy of 76.63 % and a kappa

coefficient of 0.69, and for Minimum-Distance classification an overall accuracy of 69.08 % and a kappa coefficient of 0.59. It is noted that accuracy of the building classification decreased for Maximum-Likelihood due to the missing sigma-z. The producer's accuracy for the tree classification was very high for Maximum-Likelihood and Minimum-Distance classifications.

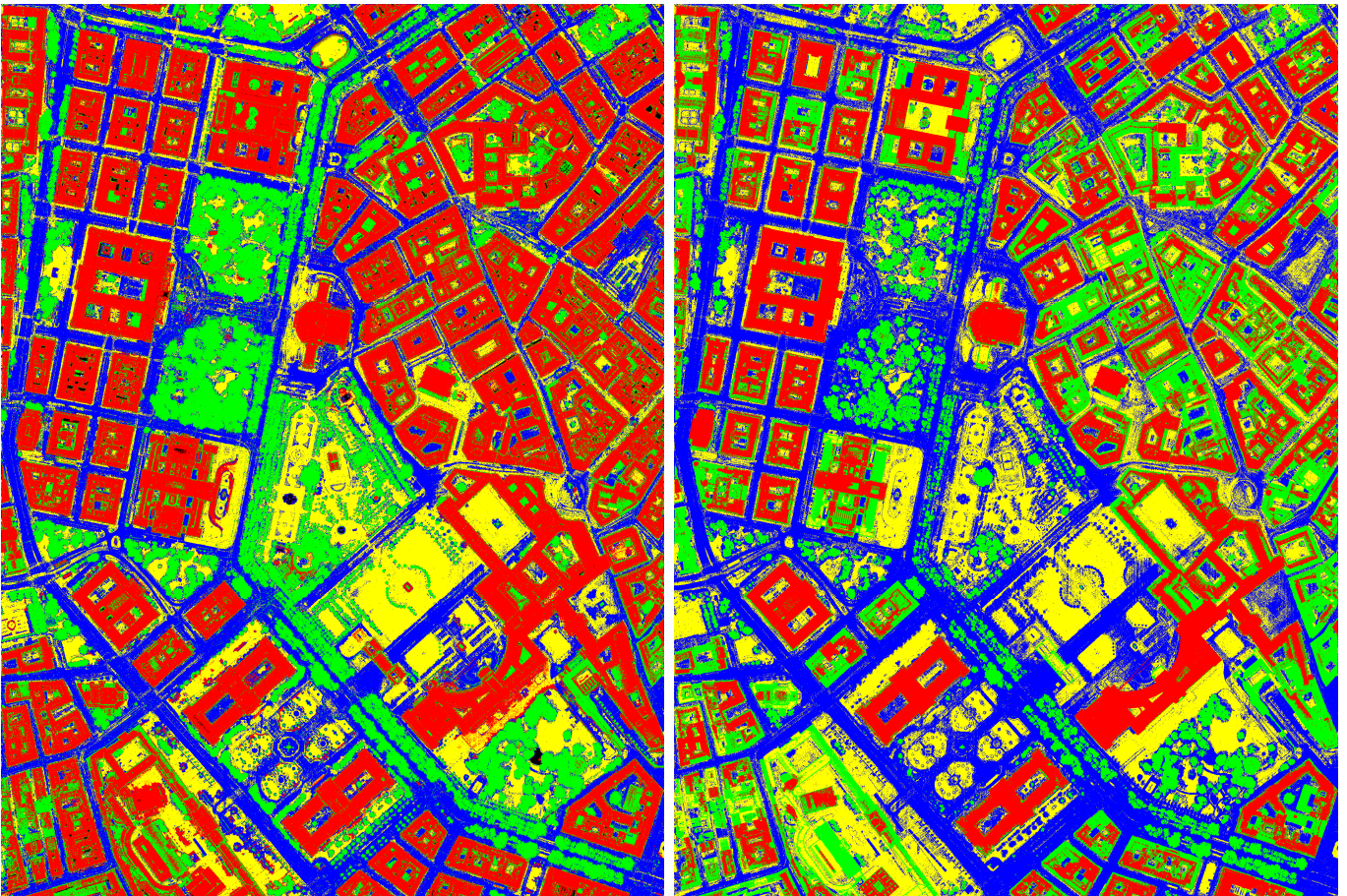
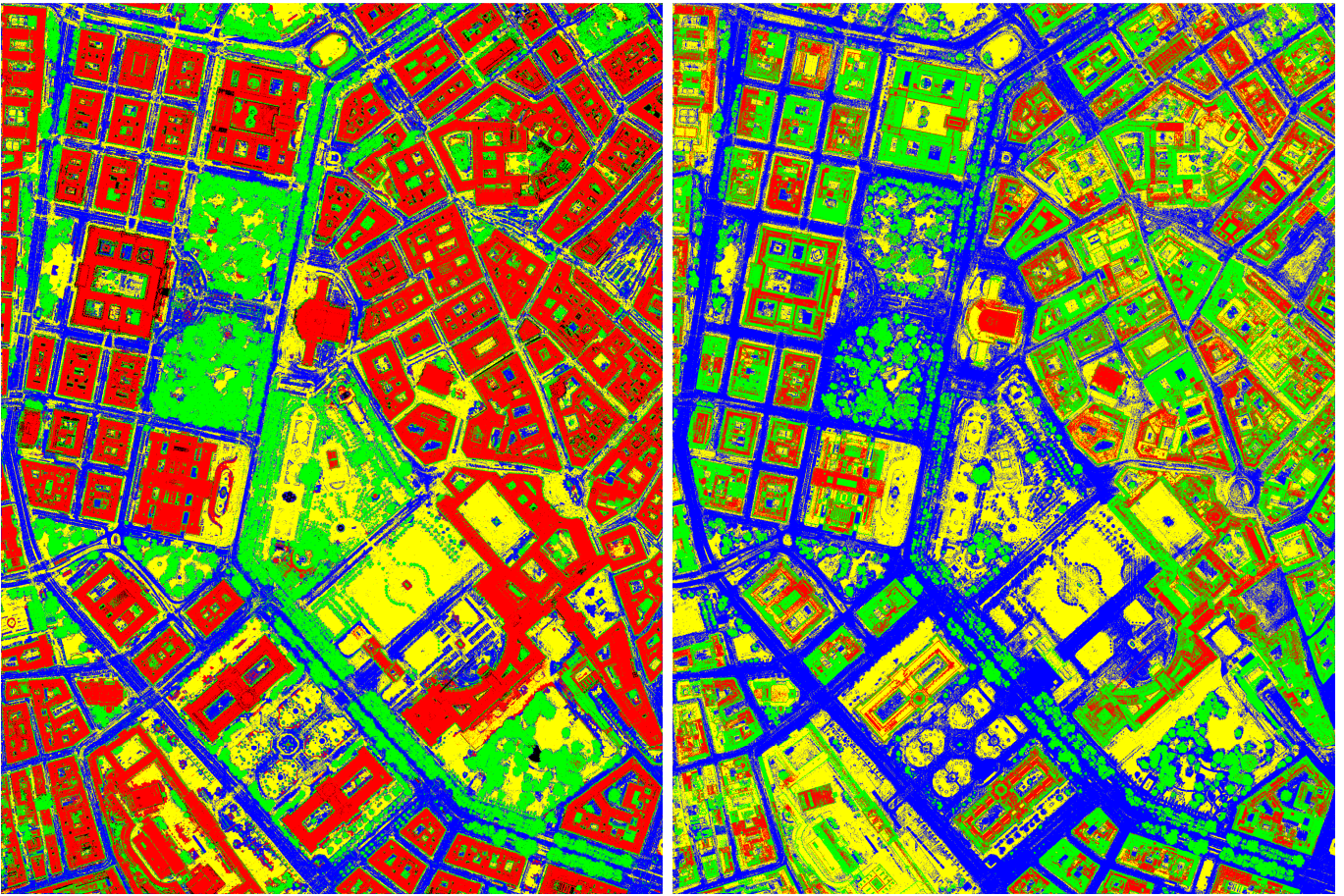
Road classification improved more than 10 % compared in the first combination for Maximum-Likelihood classification, but there is no change in the accuracy between first and second combinations for Minimum-Distance classification. Grass classification is slightly better in Minimum-Distance classification. Figure 51 shows the classification results using Maximum-Likelihood and Minimum-Distance methods.

It can be seen that the second combination gives better results for both classification methods. 47 % of buildings pixels are classified as trees using Minimum-Distance classification for the first combination, while 42 % classified as trees using Minimum-Distance for the second combination.

It is clearly noted that the Maximum-Likelihood gives more correctly classified pixels for both combinations. Because of the overlap between buildings and trees classes in most features there is difficulty in Minimum-Distance algorithm to separate correctly between these two classes. On the other hand there is more separability between road and grass classes and between grass and trees classes in most features, therefore they are more correctly classified using Minimum-Distance.

	Combinations	Class	buildings	trees	roads	grass	Total	Producer's accuracy %	User's accuracy %	Overall accuracy %
Maximum-Likelihood	First	Unclassified	551	50	107	0	708			77.10
		buildings	16452	14	418	1040	17924	80.77	91.79	
		trees	3348	7164	1289	56	11857	98.83	60.42	
		roads	12	20	11912	190	12134	58.17	98.17	
		grass	5	1	6751	11111	17868	89.63	62.18	
	Total	20368	7249	20477	12397	60491				
	Second	Unclassified	67	5	42	0	114			76.63
		buildings	14059	28	433	1007	15527	69.02	90.55	
		trees	6225	7184	1103	49	14561	99.10	49.34	
		roads	11	32	14291	519	14853	69.79	96.22	
grass		6	0	4608	10822	15436	87.30	70.11		
Total	20368	7249	20477	12397	60491					
Minimum-Distance	First	Unclassified	0	0	0	0	0			65.91
		buildings	5760	31	3	0	5794	28.28	99.41	
		trees	9651	6063	92	0	15806	83.64	38.36	
		roads	592	885	16658	1005	19140	81.35	87.03	
		grass	4365	270	3724	11392	19751	91.89	57.68	
	Total	20368	7249	20477	12397	60491				
	Second	Unclassified	0	0	0	0	0			69.08
		buildings	7493	5	2	0	7500	36.79	99.91	
		trees	8587	6249	103	0	14939	86.20	41.83	
		roads	912	800	16655	1007	19374	81.34	85.97	
grass		3376	195	3717	11390	18678	91.88	60.98		
Total	20368	7249	20477	12397	60491					

Table 7 . Error matrix of both Maximum-Likelihood and Minimum-Distance classification for two combinations.



■ Buildings
 ■ Trees
 ■ Roads
 ■ Grass

Figure 51 . Classification results of the study area, above) first combination, below) second combination. Left: Maximum-Likelihood classification, right: Minimum-Distance classification.

8.3 Decision tree classification:

To classify the entire study area using Decision Tree, all selected features used for test area are used. Also the same hierarchical created Decision Tree for test area is applied with the same thresholds of attributes used for classification (Decision tree 1) (Figure 52). This decision tree is based on 7 extracted features (nDSM, S, σ_z , Ne, min. A, min. ew, σ). Building and tree classes were classified based on five attributes nDSM, number of echoes (Ne), slope (S), sigma-z (σ_z) and minimum echo-width (min. ew). Roads and grass classes and trees (small trees and shrubs <2m) were classified based on four attributes nDSM, minimum echo-width, minimum amplitude (min. A) and cross-section (σ).

This decision tree classification gave overall accuracy of 83.16 % and kappa coefficient of 0.76 .

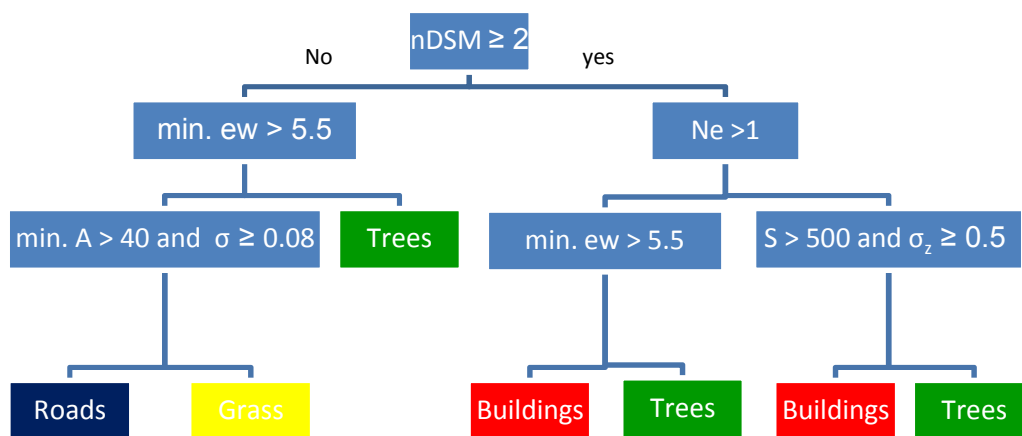


Figure 52. Decision tree used for the classification of all study area.

As we can see from the Table 8 , the producer's accuracies for buildings, tree, and road classes are more than 80 %. Grass class has the lowest value of producer's accuracy of 74.21 %.

10 % of buildings pixels were classified as trees due to the buildings edges, where Ne >1 or the echo width values for some tilted roofs are higher than 5.5 ns.

Some vehicles were classified as buildings due to their elevation above ground (nDSM > 2m). Some road areas were classified as grass due to the high values of minimum amplitude (min. A >40) and cross-section ($\sigma > 0.08$).

19 % of grass pixels were classified as roads in some areas. Figure 53 shows the classification result for study area using all selected features in the decision tree.

Class	buildings	trees	roads	grass	Total	Producer's accuracy %	User's accuracy %	Overall accuracy %
buildings	18082	418	1930	800	21230	88.78	85.17	83.16
trees	<u>2234</u>	6461	248	0	8943	89.13	72.25	
roads	47	338	16562	<u>2397</u>	19344	80.88	85.62	
grass	5	32	1737	9200	10974	74.21	83.83	
Total	20368	7249	20477	12397	60491			

Table 8. classification accuracy for the study area using Decision Tree.

As comparison between the results of test area and the entire study area we note a decline in the accuracy by using Maximum-Likelihood and Decision Tree methods. The reason could be in the training data sets and also in the features used to classify the entire area. Further investigations are recommended, which involve new training data sets and other features.

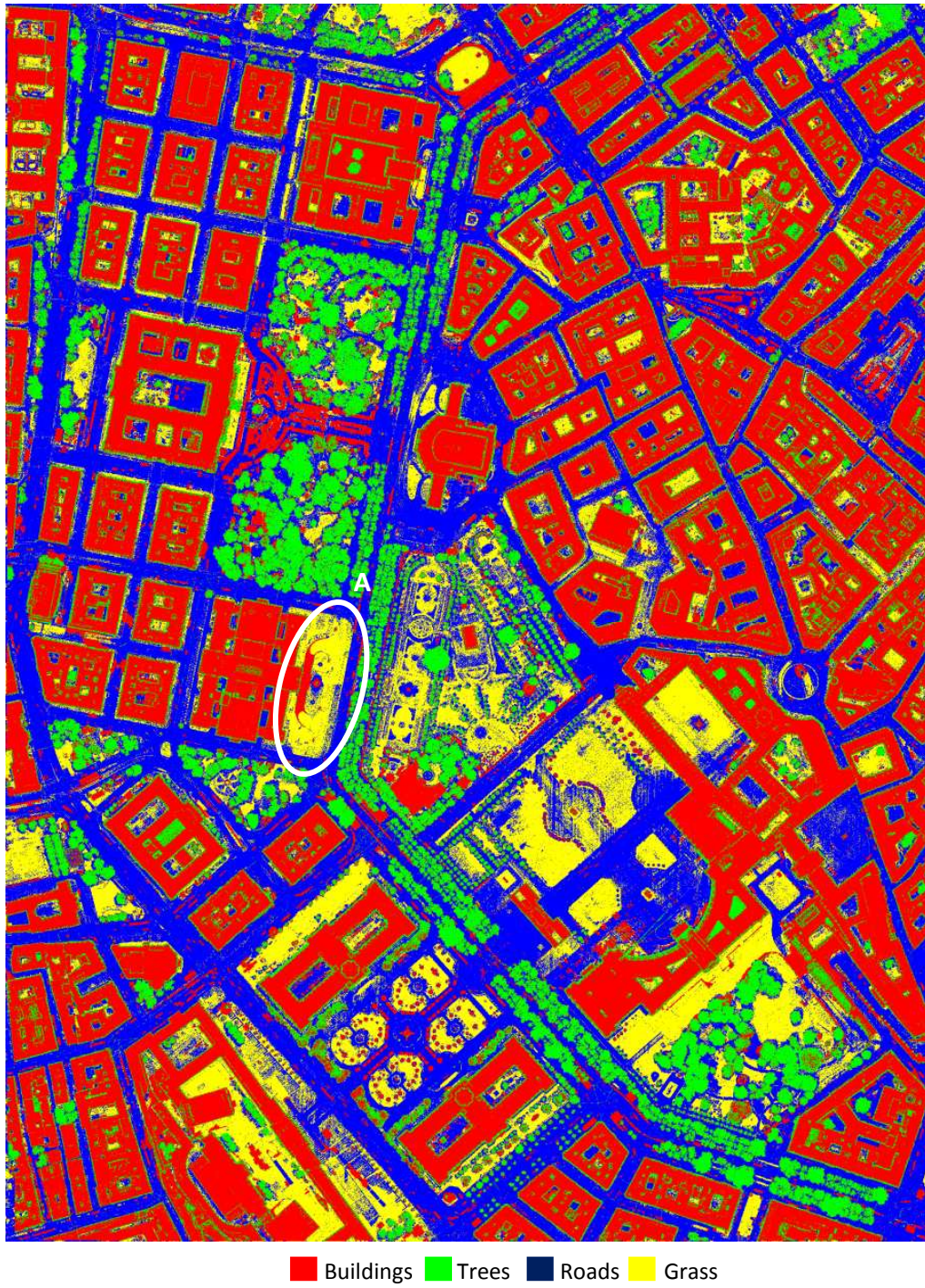


Figure 53 . Classification result of the study area using Decision Tree. A) pavements and concrete area classified as grass.

9 Conclusion and further works

This work confirms that full-waveform airborne laser scanning data could be useful for classification of urban areas. We used three classification methods, Maximum-Likelihood, Minimum-Distance and Decision Tree. The classes are buildings, trees, roads, and grass areas, which are the basic classes that could be classified in urban areas. Actually more classes can be classified (tilted roofs buildings, flat roofs, shrubs, and other classes), but our work is a first step to investigate the FWF LiDAR data classification for urban areas. Further work should focus on the discrimination of more classes. In this work we used a certain number of features extracted from FWF LiDAR data, which are normalized digital surface model, slope, sigma-z, number of echoes, minimum amplitude of the last echoes, minimum echo width of the last echoes and backscatter cross section.

Using the same extracted features, Decision Tree method gave better overall accuracy than Maximum-Likelihood and Minimum-Distance classification. Maximum-Likelihood classifications results are better than Minimum-Distance specially for buildings, trees and grass classes.

Some of used features did not contribute very much for the classification in our study area. For Maximum-Likelihood and Minimum-Distance classification, minimum amplitude (min. A) of last echoes is of less importance, although it may be responsible for a slight improvement for roads and trees. Minimum echo width (min. ew) of last echoes shows almost no influence.

But it has been seen that the minimum amplitude of the last echoes and backscatter cross-section σ are very useful for roads and grass areas classification using Decision Tree method. Also it has been seen that using backscatter cross-section σ is more useful than amplitude and echo-width in Maximum-Likelihood classifier, especially for roads classification. Thus radiometric calibration might be necessary to make any classification method effective. In our study using only Maximum-Likelihood or Minimum-Distance is not optimal for urban areas classification using only information extracted from full-waveform laser scanning data.

Further work should be carried out on different locations and should concentrate on the extraction of more useful features from FWF LiDAR data and more classes to be classified. Using aerial orthophotos combined with full-waveform airborne laser scanning data, it might be more useful for accurate classification.

Our study clearly showed that the quality of the normalized digital surface model nDSM is highly dependent on the accuracy of the digital terrain model DTM especially in urban areas. The complicated off-terrain elements are a great challenge for filter algorithms and practice proved that it is advisable to thoroughly check and if necessary correct the DTM before calculating the nDSM. A more accurate nDSM

might produce a better classification. Although the Decision Tree classifier is easy to understand and implement, the thresholds for the class discrimination are dependent on the chosen training data. Therefore, more studies are required in different locations of urban areas.

References

1. Alexander, C., Tansey, K., Kaduk, J., Holland, D., Tate, N.J., (2010). *Backscatter coefficient as an attribute for the classification of full-waveform airborne laser scanning data in urban areas*. ISPRS Journal of Photogrammetry and Remote Sensing, 65: 423-432.
2. Alexander, C., Tansey, K., Tate, N.J., Smith-Voysey, S., Kaduk, J., (2008). *Extraction of vegetation for topographic mapping from full-waveform airborne laser scanning data*. In: Hill, R., Rosette, J., Suárez, J. (Eds.), *Silvilaser 2008: 8th International Conference on Lidar Applications in Forest Assessment and Inventory*. Edinburgh, Scotland. 17-19 September. pp. 343-353.
3. Bartels, M. and Wei, H. (2006). *Maximum Likelihood Classification of LIDAR Data Incorporating Multiple Co-Registered Bands*. In: 4th International Workshop on Pattern Recognition in Remote Sensing in conjunction with the 18th International Conference on Pattern Recognition 2006, Hong Kong, 2006, 20 August 2006, 17 - 20.
4. Brennan, R., and Webster, T.L., (2006). *Object-oriented land cover classification of lidar-derived surfaces*. Canadian Journal of Remote Sensing, 32(2), pp. 162-172.
5. Baltsavias, P. E., (1999). *A comparison between photogrammetry and laser scanning*. ISPRS Journal of Photogrammetry & Remote Sensing 54 (1999), pp. 83–94.
6. Bruzzone, L., Wegmüller, U., Wiesmann, A. (2004). *An advanced system for the automatic classification of multi temporal SAR images*. IEEE Transactions on Geoscience and remote sensing, Vol. 42, NO. 6.
7. Briese, Ch., Pfeifer, N., (2001). *Airborne laser scanning and derivation of digital terrain models*. In: Gruen, A., Kahmen, H. (Eds.), *Optical 3D Measurement Techniques V*. Technical University, Vienna, Austria, pp. 80– 87.
8. Brenner, C. (2006). *International Summer School “Digital Recording and 3D Modeling”*, Aghios Nikolaos, Crete, Greece, 24-29 April 2006.
9. Charaniya, P. A., Roberto, M., and Lodha, K. S. (2004). *Supervised parametric classification of aerial lidar data*. Computer Vision and Pattern Recognition Workshop, pp. 25–32, 2004.
10. Clode, S. P., Rottensteiner, F., Kootsookos, P., Zelniker, E. (2007). *Detection and vectorisation of roads from LIDAR data*. Photogrammetric Engineering & Remote Sensing 73(5): 517-536.
11. Chehata, N., Guo, L. Mallet, C., (2009). *Airborne lidar featureselection for urban classification using random forests*. Laser scanning 2009, IAPRS, Vol. XXXVIII, Part 3/W8- Paris, France, September 1-2, 2009.

12. Chen, Y., Su, W., Li, J., Sun, Z., (2009). *Hierarchical object oriented classification using very high resolution imagery and LIDAR data over urban areas*. Advances in space research 43, pp. 1101-1110.
13. Carlberg, M., Gao, P., Chen, G. and Zakhor, A., (2009). *Classifying urban landscape in aerial LiDAR using 3D shape analysis*. In: IEEE International Conference on Image Processing, Cairo, Egypt, pp. 1701–1704.
14. Ducic, V., Hollaus, M., Ullrich, A., Wagner, W., Melzer, T., (2006). *3D vegetation mapping and classification using full-waveform laser scanning*. In: Proc. Workshop on 3D Remote Sensing in Forestry. EARSeL/ISPRS, Vienna, Austria, 14-15 February 2006, pp. 211-217.
15. Dinis, J., Navarro, A., Soares, F., Santos, T., Freire, S., Fonseca, A., Afonso, N., Tenedório, J., (2010). *Hierarchical object-based classification of dense urban areas by integrating high spatial resolution satellite images and lidar elevation data*. The International Archives of the Photogrammetry, Remote Sensing and Spatial Information Sciences, Vol. XXXVIII-4/C7.
16. Frauman, E., Wolff, E. (2005). *Change detection in urban areas using very high spatial resolution satellite images*. Libre University, Brussels.
17. Gross, H., Jutzi, B., and Thoenessen, U., (2007). *Segmentation of tree regions using data of a full-waveform laser*. In International Archives of Photogrammetry, Remote Sensing and Spatial Information Sciences, volume 36 (Part 3/W49A), pages 57-62, Munich, Germany.
18. Grey, W., Luckman, A., (2003). *Mapping urban extent using satellite Radar Interferometry*. Photogrammetric Engineering & Remote Sensing, Vol. 69, NO. 9, pp. 957-961.
19. Guo, L., Chehata, N., Mallet, C., Boukir, S., (2010). *Relevance of airborne lidar and multispectral image data for urban scene classification using Random Forests*. ISPRS Journal of Photogrammetry and Remote Sensing, Vol. 66, pp. 56-66.
20. Herold, M., Liu, X., Clarke, C. K., (2003). *Spatial Metrics and Image Texture for Mapping Urban Land Use*. Photogrammetric Engineering & Remote Sensing, Vol. 69, NO. 9, pp. 991-1001.
21. Hollaus, M., Mandlburger, G., Pfeifer, N., Mücke, W., (2010). *Land cover dependent derivation of digital surface models from airborne laser scanning data*. IAPRS, Vol. XXXVIII, Part 3A- Saint-Mande, France, September 1-3, 2010.
22. Höfle, B., Hollaus, M., (2010). *Urban vegetation detection using high density full-waveform airborne lidar data – Combination of object-based image and point cloud analysis*. ISPRS TC VII Symposium, 100 years ISPRS, Vienna, Austria, July 5-7, IAPRS, Vol. XXXVIII, Part 7B.
23. Jansa, J., Studnicka, N., Forkert, G., Haring, A., Kager, H. (2004). *Terrestrial laser scanning and photogrammetry acquisition techniques complementing one*

- another*. The International Archives of the Photogrammetry, Remote Sensing and Spatial Information Sciences, Vol. 34, Part XXX.
24. Jansa, J. Wagner, W. (2011). Advances in laser scanning. Turkish National Society for Photogrammetry and Remote Sensing, 6th Technical Symposium, 23-26 February, 2011.
 25. Jensen, R. J., Cowen, C. D., (1999). *Remote sensing of urban/suburban infrastructure and socio-Economic attributes*. Photogrammetric Engineering & Remote Sensing, Vol. 65, NO. 5, pp. 611-622.
 26. Jutzi, B., and Stilla, U., (2003). *Laser pulse analysis for reconstruction and classification of urban objects*. In International Archives of Photogrammetry, Remote Sensing and Spatial Information Sciences, volume 34 (Part 3/W8), pages 151-156, Munich, Germany.
 27. Jutzi, B., and Stilla, U., (2005). *Waveform processing of laser pulses for reconstruction of surfaces in urban areas*. In International Archives of Photogrammetry, Remote Sensing and Spatial Information Sciences, volume 36 (Part 8/W27), Tempe, AZ, USA.
 28. Kraus, K. and Pfeifer, N., (1998). *Determination of terrain models in wooded areas with airborne laser scanner data*. ISPRS Journal of Photogrammetry and Remote Sensing, 53:193–203.
 29. Kager, H. (2005). *Quality check and georeferencing of aerial laser scanner strips*. Vienna University of Technology, Institute of Photogrammetry and Remote Sensing.
 30. Lin, C. Y., Mills, P. J. (2009). *Integration of full-waveform information into the airborne laser scanning data filtering process*. ISPRS, Vol. XXXVIII/3-W8, 2009.
 31. Lohr, U. (2003). *Precision LIDAR Data und True-Ortho Images*. Map Asia Conference 2003.
 32. Lillesand, M. T., Kiefer, W. R., Chipman, W. J., (2004). *Remote Sensing and Image Interpretation*. Fifth edition, USA. John Wiley & Sons.
 33. Lehner, H., Briese, Ch., (2010). *Radiometric calibration of full-waveform airborne laser scanning data based on natural surfaces*. ISPRS TC VII Symposium, 100 years ISPRS, Vienna, Austria, July 5-7, IAPRS, Vol. XXXVIII, Part 7B.
 34. Mallet, C., Soergel, U., Bretar, F., (2008). *Analysis of full-waveform lidar data for an accurate classification of urban areas*. International Archives of Photogrammetry, Remote Sensing and Spatial Information Sciences 37 (Part 3A), 85-92.
 35. Mallet, C., Bretar, F., (2009). *Full-waveform topographic lidar: state-of-the-art*. ISPRS Journal of Photogrammetry and Remote Sensing 64 (1), 1–16.
 36. Mandlbürger, G., Otepka, J., Karel, W., Wagner, W., Pfeifer, N., (2009). *Orientation and processing of airborne laser scanning data OPALS—concept and first results of a comprehensive ALS software*. International Archives of

- Photogrammetry, Remote Sensing and Spatial Information Sciences 38 (Part 3/W8), 55–60.
37. Mallet, C., Bretar, F., Soergel, U., (2008). *Analysis of Full-Waveform Lidar Data for Classification of Urban areas*. Photogrammetrie - Fernerkundung - Geoinformation, vol. 5, pp. 337-349, 2008.
 38. Matikainen, L., Kaartinen, H., Hyyppä, J., (2007). *Classification tree based building detection from laser scanner and aerial image data*. ISPRS Workshop on laser scanning 2007 and SilviLaser 2007, Espoo, September 12-14, 2007, Finland.
 39. Mallet, C. (2010). *Analysis of full-waveform lidar data for urban area mapping*. Dissertation for Doctoral thesis, Paris, France.
 40. Mancini, A., Frontoni, E., Zingaretti, P., (2009). *Automatic extraction of urban objects from multi-source aerial data*. IAPRS, Vol. XXXVIII, Part 3/W4, Paris, France, 3-4 September, 2009.
 41. Pfeifer, N., Briese, Ch., (2007). *Laser scanning – Principles and Applications*. 3rd International Exhibition & Scientific Congress on Geodesy, Mapping, Geology, Geophysics, Cadaster GEO-SIBERIA 2007, Novosibirsk, Russia.
 42. Pfeifer, N., Stadler, P., Briese, C., (2001). *Derivation of Digital Terrain Models in the SCOP++ Environment*. In OEEPE workshop on Airborne Laser scanning and Interferometric SAR for Detailed Digital Terrain Models, Stockholm, 2001.
 43. Rutzinger, M., Höfle, B., Pfeifer, N., (2007). *Detection of high urban vegetation with airborne laser scanning data*. In: Proceedings Forestsat 2007. Montpellier, France, pp. 1-5.
 44. Rönnholm, P., Honkavaara, H., Litkey, P., Hyyppä, H., Hyyppä, J. (2007). *Integration of laser scanning and Photogrammetry*. IAPRS, Vol. XXXVI, Part 3/W52, 2007.
 45. Rottensteiner, F., J. Trinder, S. Clode, and K. Kubik, (2003). *Building detection using LIDAR data and multispectral images*. Proceedings of DICTA, Sydney, Australia, Vol. 2, pp. 673–682.
 46. Rutzinger, M., Höfle, B., Hollaus, M., Pfeifer, N., (2008). *Object-based point cloud analysis of full-waveform airborne laser scanning data for urban vegetation classification*. Sensors 8 (8), 4505–4528.
 47. Sithole, G., Vosselman, G., (2006). *Bridge detection in airborne laser scanner data*. ISPRS Journal of Photogrammetry and Remote Sensing, 61(1):33-46, 2006.
 48. Sithole, G., Vosselman, G., *Automatic structure detection in a point-cloud of an urban landscape*. 2th GRSS/ISPRS Joint workshop on "Data fusion and remote sensing over urban areas".
 49. Shan, J., Toth, K. Ch. (2008). *Topographic laser ranging and scanning*. USA, Taylor & Francis Group.
 50. Samadzadegan, F., Bigdeli, B. and Hahn, M., (2009). *Automatic road extraction from lidar data based on classifier fusion in urban area*. In International

Archives of Photogrammetry, Remote Sensing and Spatial Information Sciences 38 (Part 3), pp. 81–87.

51. Tooke, R. T., Coops, C. N., Goodwin, R. N., Voogt, A. J., (2009). *Extracting urban vegetation characteristics using spectral mixture analysis and decision tree classifications*. Remote Sensing of Environment 113 (2009) 398–407.
52. Tarsha-Kurdi, F., Landes, T., Grussenmeyer, P. and Smigiel, E., (2006). *New approach for automatic detection of buildings in airborne laser scanner data using first echo only*. IAPRS Vol. 36, part. 3, pp. 25-30.
53. Tupin, F., Haushmand, B., Datcu, M. (2002). *Road detection in dense urban areas using SAR imagery and the usefulness of multiple views*. IEEE Transactions on Geoscience and remote sensing, Vol. 40, NO. 11.
54. Vosselman, G. (2000). *Slope based filtering of laser altimetry data*. In International Archives of Photogrammetry and Remote Sensing, Vol. XXXIII, Part B3 , pages 935–942, Amsterdam, Netherlands.
55. Wagner, W., Ullrich, A., Ducic, V., Melzer, T., Studnicka, N., (2006). *Gaussian decomposition and calibration of a novel small-footprint full-waveform digitizing airborne laser scanner*. ISPRS Journal of Photogrammetry and Remote Sensing 60 (2), 100–112.
56. Wagner, W., Hollaus, M., Briese, C., Ducic, V., (2008a). *3D vegetation mapping using small-footprint full-waveform airborne laser scanners*. International Journal of Remote Sensing 29 (5), 1433-1452.
57. Wagner, W. (2010). *Radiometric calibration of small-footprint full-waveform airborne laser scanner measurements: Basic physical concepts*. ISPRS Journal of Photogrammetry and Remote Sensing, 65: 505-513.
58. Wagner, W., Roncat, A., Melzer, T., Ullrich, A., (2007). *Waveform analysis techniques in airborne laser scanning*. IAPRS Vol. XXXVI, part 3/W52, 2007.
59. Wagner, W., Hyypä, J., Ullrich, A., Lehner, H., Briese, Ch., Kaasalainen, S. (2008). *Radiometric calibration of full-waveform small-footprint airborne laser scanners*. The International Archives of the Photogrammetry, Remote Sensing and Spatial Information Sciences. Vol. XXXVII. Part B1. Beijing 2008.
60. Zhan, Q.; Molenaar, M.; Tempfli, K. (2002). *Hierarchical image-object based structural analysis toward urban land use classification using high-resolution imagery and airborne LIDAR data*. In: *Proceedings of the 3rd International Symposium on Remote Sensing of Urban Areas, Istanbul, Turkey, June 11-13 (2002)*. - [S.l.] : [s.n.], 2002 - p. 251 - 258.
61. Zaletnyik, P., Laky, S., Toth, C., (2010). *Lidar waveform classification using self-organizing map*. ASPRS 2010, annual conference, April 26-30, San Diego, California.

WWW References and Software help:

62. <http://www.wieninternational.at/de/node/2846> (Access: 8/02/2011)
63. www.riegl.com
64. Opals help... (2010)
65. <http://www.wien.gv.at/stadtentwicklung/stadtvermessung>. (Access: 19/12/2010)
66. <http://www.optech.ca/altmhow.htm> (Access: 12/02/2011)
67. <https://www.e-education.psu.edu/lidar/book/export/html/1798>. (Access: 15/3/2011).
68. ENVI help, version 4.4.
69. SCOP++ help, version 5.4.

Curriculum Vitae

Personal Data

Name: Sharif Hasan

Date of Birth: 27. 03. 1981

Birthplace: Safita, Syria

Citizenship: Syrian

Education

1987-1993 Primary school, Tartous, Syria

1993-1996 Middle school, Tartous, Syria

1996-1999 High school, Tartous, Syria

1999-2004 University study at Damascus University (Damascus, Syria)

Field: Civil Engineering

2009-2011 Master study at the Technical University of Vienna (TU Vienna)

Field: Geoinformation

